



# Membranes composed of poly(lactic acid)/poly(ethylene glycol) and Ora-pro-nóbis (*Pereskia aculeata* Miller) extract for dressing applications

Juliana Farinassi Mendes<sup>a,\*</sup>, Marina de Lima Fontes<sup>b</sup>, Talita Villa Barbosa<sup>c</sup>,  
Rafaella T. Paschoalin<sup>a</sup>, Luiz Henrique Capparelli Mattoso<sup>a</sup>

<sup>a</sup> National Laboratory of Nanotechnology for Agriculture (LNNA), Embrapa Instrumentation, São Carlos 13560-970, São Paulo, Brazil

<sup>b</sup> Graduate of Pharmaceutical Sciences, Paulista State University, Araraquara 14800-901, São Paulo, Brazil

<sup>c</sup> São Carlos School of Engineering, University of São Paulo, 13560-970 São Carlos, São Paulo, Brazil

## ARTICLE INFO

### Keywords:

Nanofibers  
Solution-blow-spinning (SBS)  
Antioxidant activity  
Swelling tests  
Cell viability  
Tissue engineering

## ABSTRACT

Wounds are considered one of the most critical medical conditions that must be managed appropriately due to the psychological and physical stress they cause for patients, as well as creating a substantial financial burden on patients and global healthcare systems. Nowadays, there is a growing interest in developing nanofiber mats loaded with varying plant extracts to meet the urgent need for advanced wound dressings. This study investigated the development and characterization of poly(lactic acid) (PLA)/ poly(ethylene glycol) (PEG) nanofiber membranes incorporated with Ora-pro-nóbis (OPN; 12.5, 25, and 50 % w/w) by the solution-blow-spinning (SBS) technique. The PLA/PEG and PLA/PEG/OPN nanofiber membranes were characterized by scanning electron microscopy (SEM), thermal properties (TGA and DSC), Fourier transform infrared spectroscopy (FTIR), contact angle measurements and water vapor permeability (WVTR). In addition, the mats were analyzed for swelling properties in vitro cell viability, and fibroblast adhesion (*L-929*) tests. SEM images showed that smooth and continuous PLA/PEG and PLA/PEG/OPN nanofibers were obtained with a diameter distribution ranging from 171 to 1533 nm. The PLA/PEG and PLA/PEG/OPN nanofiber membranes showed moderate hydrophobicity (~109–120°), possibly preventing secondary injuries during dressing removal. Besides that, PLA/PEG/OPN nanofibers exhibited adequate WVTR, meeting wound healing requirements. Notably, the presence of OPN gave the PLA/PEG membranes better mechanical properties, increasing their tensile strength (TS) from 3.4 MPa (PLA/PEG) to 5.3 MPa (PLA/PEG/OPN), as well as excellent antioxidant properties (Antioxidant activity with approximately 45 % oxidation inhibition). Therefore, the nanofiber mats based on PLA/PEG, especially those incorporated with OPN, are promising options for use as antioxidant dressings to aid skin healing.

## 1. Introduction

In recent decades, biopolymeric nanofiber membranes have gained significant interest in wound dressing applications due to their advantages as drug-release devices and suitable substrates for cell adhesion and proliferation [1–5]. Nanofibers exhibit properties that promote hemostasis, fluid absorption, cell respiration, and gas permeation, making them effective in accelerating the healing process, reducing pollution, and treating infections [6]. These benefits are attributed to their unique characteristics, including nanometer-scale diameter, large specific surface area, high load capacity, and high porosity with good pore interconnectivity [7,8]. Additionally, nanofibers offer mechanical and barrier properties suitable for human cells, promoting a more

effective regeneration process of the new extracellular matrix (ECM) [9].

Solution blow spinning (SBS), an innovative technology for fabricating nanofibers [10–13], is increasingly recognized for its potential in various applications, such as biomedical engineering [14], food packaging [14], flexible sensors [15], thermal conductivity [16], and filtration [17]. SBS offers several advantages over electrospinning [18], such as not requiring high voltage or specific collectors, and providing high production yields [19]. In the SBS process, a polymer solution or suspension is fed through a nozzle, with pressurized air simultaneously flowing along the nozzle outer channel. The air flow ejects the polymer jet and accelerates solvent removal during nanofiber formation. Introduced in 2009, SBS has been optimized to obtain fibrous membranes

\* Corresponding author.

E-mail address: [julianafarinassi@gmail.com](mailto:julianafarinassi@gmail.com) (J.F. Mendes).

<https://doi.org/10.1016/j.ijbiomac.2024.131365>

Received 13 November 2023; Received in revised form 28 March 2024; Accepted 2 April 2024

Available online 5 April 2024

0141-8130/© 2024 Elsevier B.V. All rights reserved.

from synthetic polymers and other materials [20–26]. While most studies use electrospinning develop nanofibers for dressings, this study stands out by using SBS [1,27–34]. SBS applications, particularly in the biomedical field, are significant due to its ability to directly apply fibrous material to target sites, such as on the body or in wounds.

PLA (polylactic acid) is an essential biopolymer widely used in tissue engineering, especially for wound dressing applications [35,36]. It is derived from renewable plant sources and boasts attributes such as biodegradability, processing versatility, and FDA approval for human contact [37–39]. However, its hydrophobic nature may limit cell adhesion. Poly(ethylene glycol) (PEG) is known for its biocompatibility, flexibility, and hydrophilic character, making it a suitable candidate for blending with PLA to control nanofiber properties [40,41]. Despite the difficulties on blending PEG and PLA due to their different natures that cause phase separation, the SBS timeframe does not allow complete phase separation so tailor-made formulations are feasible. Several studies have explored polymeric mixtures incorporating PEG or surface modification, and encapsulated bioactive compounds with antioxidant and/or antimicrobial properties to overcome these limitations [3,38,42,43]. Furthermore, PLA biopolymer utilization in nanofiber production is promising in encapsulating and controlling bioactive compounds release, regulating the leaching rate through interactions with the polymeric matrix [44].

Natural products with notable healing properties, potential antimicrobial and/or antioxidant effects, have been widely utilized to expedite the wound healing process, as extensively documented in the literature [14,16,38,41,45,46]. One of these natural resources is the *Pereskia aculeata* Miller (*P. aculeata*) extract, commonly known as Ora-pro-nóbis (OPN), belonging to the Cactaceae family and Pereskioideae subfamily, native to tropical America and Brazil. OPN has been extensively employed as a medicinal plant due to its diverse properties, including antibacterial, antiviral, and anti-inflammatory effects [2,47]. It is also valued for its nutritional content, containing significant amounts of protein, minerals, dietary fibers, and vitamins. Several studies have highlighted OPN's diverse phenolic composition, including phenolic acids, flavan-3-ols, quercetin, and myricetin, among others [2,48–50]. Caffeic acid is the most prevalent phenol, followed by catechin and quercetin, exhibiting potent antioxidant, anti-inflammatory, and antimicrobial activities [2,48–50]. Pinto et al. [51] identified additional phenolics such as tryptamine, abrine, mescaline, hordenine, petunidin, and isomers of di-tert-butylphenol. Moreover, OPN contributes to wound healing, alleviates inflammatory processes, and supports skin burn recovery [52]. When applied topically, quercetin has been suggested to serve as an excellent protective agent against diseases caused by oxygen-free radicals and demonstrates anti-lipoperoxidative activity [53–55]. Also, OPN has been utilized as reinforcement in bacterial cellulose films, enhancing their resistance compared to control films, as observed in previous research.

Numerous researchers have explored the effects of herbal extracts on nanofibers, investigating their physical-mechanical and biological properties for biomedical purposes such as wound dressings and drug delivery systems. Uddin et al. [56] incorporated various extracts, including nigella, honey, garlic, and olive, into a PVA solution, from which nanofibers were produced for biomedical applications. The resulting PVA/nigella/honey (PNH) and PVA/garlic/honey/olive oil (PGHO) nanofibers exhibited inhibition zones against *S. aureus* bacteria measuring 36 mm and 35 mm, respectively. However, no studies to date have been found in the literature regarding OPN-incorporated nanofibers production for wound dressing applications, despite numerous studies highlighting OPN's antioxidant and anti-inflammatory properties.

The novelty of this study lies in utilizing SBS as an alternative technique for producing PLA/PEG nanofibers. Additionally, OPN extract was incorporated into PLA/PEG biopolymers to manufacture nanofibers by SBS, focusing on wound healing applications. Therefore, this study aimed to develop and characterize PLA/PEG nanofiber membranes

incorporated with different OPN concentrations (12.5, 25, and 50 % w/w) using the SBS technique. OPN components' incorporation performance on the main PLA/PEG nanofibers was addressed by characterizing the morphology with scanning electron microscopy (SEM), physicochemical properties with Fourier Transform Infrared Spectroscopy (ATR-FTIR) and X-ray diffraction (XRD), thermal properties (thermogravimetric analysis -TGA and differential scanning calorimetry -DSC), mechanical and antioxidant properties, contact angle measurements, water vapor permeability (WVTR) and swelling properties. Cell viability, adhesion, and fibroblasts proliferation (*L-929*) on the nanofiber membranes' surface were investigated to assess the applicability of PLA/PEG and PLA/PEG/OPN nanofibers in dressings.

## 2. Materials and methods

### 2.1. Materials

Poly(lactic acid) (PLA) (Molecular Weight: 66,000 g.mol<sup>-1</sup>) and poly(ethylene glycol) (PEG) (Molecular Weight: 8000 g.mol<sup>-1</sup>) were obtained from Nature Works (Minnesota, EUA) and Sigma Aldrich (St. Louis, MO, USA), respectively. The Ora-pro-nóbis (*Pereskia aculeata* Miller) (OPN) leaves used to prepare the extract were purchased in São Carlos-SP, Brazil. Chloroform and acetone were purchased from Synth (Rio de Janeiro, Brazil) and were not purified. Phosphate-buffered saline (PBS) at pH 7.4 was used for the swelling and release tests.

### 2.2. Obtaining OPN mucilage

SBS preparation process is shown in Fig. 1A. The OPN mucilage obtaining-process was conducted following the methodology by Neves et al. [57], with modifications. Initially, OPN was extracted by grinding 1 kg of leaves with 2.5 L of boiling water in a blender for 10 min. The mixture was heated to 75 °C using a thermostatic bath (Quimis q-215-2, SP, Brazil) for 6 h. The mixture was vacuum-filtered using three layers of organza cloth. The filtrate was then centrifuged for approximately 10 min at 8000 rpm to remove as much mucilage as possible. The supernatant, along with the centrifuged material were placed in Petri dishes and a forced-air oven (Marconi, Piracicaba, SP, Brazil) at 40 °C until completely dry. The resulting powder was ground using a pistil.

### 2.3. OPN chemical composition

The lipid content's chemical analysis was determined according to the Ai3-75 procedure by the Soxhlet method using petroleum ether [58]. Moisture, ash, protein, and total fiber contents were determined following the Association of Official Analytical Chemistry's procedures [58]. The moisture content was measured in an oven at 105 °C for 24 h (AOAC Official Method 934.01 [59]), and the ash content was measured in a muffle at 550 °C until obtaining white or slightly grey ashes (Method 923.03) [58]. Micro-Kjeldahl was used to determine total nitrogen, and the protein amount was converted using a 6.25 conversion factor (method 981.10) [58]. The total carbohydrate content was obtained by difference, adding the contents of the previous determinations (moisture, protein, lipid, and ash) and decreasing this value from 100 %. All analyses were performed in triplicate. The results were expressed in grams per 100 g dry basis. OPN was also characterized regarding its Lignin content – ABNT [60]; Holocellulose (cellulose + hemicellulose) – Rebenfeld [61]; Cellulose – White [62].

### 2.4. Method

The SBS preparation process is shown in Fig. 1B. First, PLA (2.24 g) was dissolved in chloroform: acetone solvent mixture (3:1 v/v; 16 mL total volume) at room temperature. The chloroform: acetone (3:1) solvent mixture was used to form uniform nanofibers without defects, avoiding drops forming in the structure [63,64]. Subsequently, 10 %

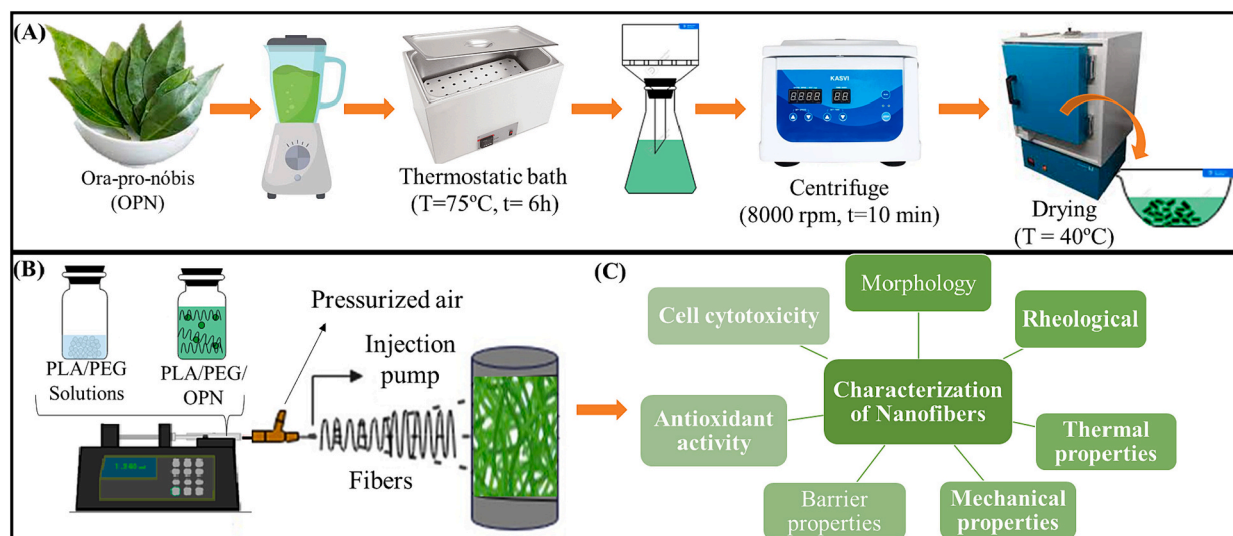


**Fig. 1.** Experimental procedures diagrams for (A) Obtaining OPN mucilage. (B) Solution-blow-spinning (SBS) process for poly(lactic acid) (PLA)/ poly(ethylene glycol) (PEG) nanofibers obtaining, influenced by varying Ora-pro-nóbis (OPN; 12.5, 25, and 50 % w/w). (C) Nanofibers characterization.

PEG was added relative to the PLA mass - and stirring for 3 h. The incorporated PEG concentration was established as per studies by Moradkahneshad et al. [8], Riley et al. [65] and Mendes et al. [66]. The blend concentration was consistently maintained at 12 % for all solutions, as established in previous studies by our research group [3,15]. To prepare SBS solutions containing OPN, PLA/PEG solution's (12 % w/v) and different OPN concentrations (12.5, 25, and 50 % w/w based on the solution's solid content) were dissolved in a mixed solvent (chloroform: acetone, 3:1 by volume) and stirred at room temperature for approximately 4 h until a homogeneous solution was obtained. OPN content was pre-determine Fig. S1A shows that, the color of the nanofiber was too light to be observed when the OPN content was at 10 %. Fig. S2B shows that the OPN could not be completely dissolved in the solution and the nanofibers' surface color was not uniform when the OPN content was at >50 %. Thus, different nanofibers incorporated with 12.5 %, 25 % and 50 % OPN were prepared. The nanofibers with 0 %, 12.5 %, 25 % and 50 % m/m, (based on the PLA and PEG mass) were named PLA/PEG, PLA/PEG/OPN12.5 %, PLA/PEG/OPN25% and PLA/PEG/OPN50%, respectively.

The PLA/PEG and PLA/PEG/OPN polymeric solutions (at 12.5 %, 25 %, and 50 % w/w concentrations) were individually transferred to 25 mL syringes. They were subsequently used to produce nanostructured membranes by SBS. The solutions in the syringes were then connected to a syringe pump (NE-300 Higher Pressure Syringe Pump, New Era, Rio de Janeiro-RJ) and adjusted to 7.0 mL.h<sup>-1</sup> flow rate. A needle was inserted into a concentric nozzle system consisting of a 0.5 mm diameter inner nozzle and an outer nozzle through which pressurized air passed at a 1.0 kPa pressure rate. The working distance between the needle and the collector was 25 cm. The resulting fibers were deposited directly on the aluminum surrounding the collector, at 180 rpm rotation speed. After that the obtained nanofiber membranes were placed in a desiccator to remove the residual solvent. Finally, morphological, physical, mechanical, and biological properties were investigated in PLA/PEG and PLA/PEG/OPN nanofibers membranes for wound healing applications.

## 2.5. Nanofibers characterization

### 2.5.1. Rheological characterization

PLA/PEG and PLA/PEG/OPN (12.5, 25, and 50 % w/w) viscosity was measured using an MCR 302 rheometer from Anton Paar, Austria. A concentric cylinder geometry (DB26.7/QI) 28- and 30-mm diameter was employed and maintained at 25 °C. The samples were allowed to

equilibrate for 1 min to eliminate any potential influence from previous shear history. The viscosity was measured for shear rates ranging from 10<sup>0</sup> to 10<sup>3</sup> s<sup>-1</sup>. A 0.1–100 rad/s frequency sweep at 190 °C was performed on all samples under a constant 0.01 % strain (within the linear viscoelastic region (LVR)).

### 2.5.2. Nanofibers morphology

The nanofibers morphology was analyzed using Scanning Electron Microscopy (SEM) at a 10 kV accelerating voltage using a JEOL JSM-6510 instrument. Before imaging, all nanofiber samples underwent gold-coating (Balzer, SCD 050). The nanofibers diameter was determined directly from SEM images using ImageJ software and 150 fibers randomly chosen from the SEM images were utilized in this analysis. To observe the samples's elemental compositions, the SEM operated at a 15 kV accelerating voltage and equipped with an Energy Dispersive Spectrometer (EDS). Before SEM-EDS imaging, all samples were coated with a thin layer of carbon.

### 2.5.3. Fourier transform infrared spectroscopy (FTIR)

Fourier Transform Infrared Spectroscopy measurements were obtained using an FTIR model Vertex 70 Bruker spectrophotometer (Bruker, Germany). Spectra were recorded at a spectral range between 4000 and 400 cm<sup>-1</sup> at a 128-scans rate and a 2 cm<sup>-1</sup> spectral resolution. The FTIR spectrum was employed in the diamond crystal and ATR module. The analyses were performed to study the effect of adding OPN in PLA/PEG, and to verify possible PLA, PEG, and OPN interactions.

### 2.5.4. Thermal properties

The thermal properties assessed the PLA/PEG nanofiber samples' thermal stability with or without OPN incorporation, which were studied by thermogravimetric analysis (TG) and differential scanning calorimetry (DSC). The thermal degradation profiles of PLA/PEG and PLA/PEG/OPN (12.5, 25 and 50 % w/w) nanofibers (approximately 6 mg) were obtained using a TGA Q500 (TA Instruments, New Castle, USA) from 25 to 600 °C at 10 °C.min<sup>-1</sup> in a synthetic air atmosphere. The onset temperature (Td,onset) and stabilization temperature (Td,offset) were determined according to the ASTM E2550 standard [67]. Td,onset was identified on the TGA curve when a deviation from the established baseline occurred, indicating the start of sample thermal decomposition. Td,offset corresponds to the point where the sample decomposition rate decreases significantly or stabilizes after reaching the maximum.

The nanofiber samples' thermal properties were further assessed

using Differential Scanning Calorimetry (DSC, TA Instrument, Q100, Newcastle, USA). Measurements were performed using 5–6 mg samples, sealed in an aluminum pan, and heated from 0 to 180 °C at 10 °C.min<sup>-1</sup>. Crystallinity index (CI(%)) was determined from the DSC curves and calculated using Eq. 1:

$$CI(\%) = \frac{\Delta Hm - \Delta Hc}{\Delta Hm^{PLA,0} \times W^{PLA}} \times 100 \quad (1)$$

where  $\Delta Hm$  is the sample's fusion enthalpy,  $\Delta Hc$  is the cold crystallization enthalpy,  $\Delta Hm^{PLA,0}$  is the fusion enthalpy based on 100 % crystalline PLA (93 J/g) [3], and  $W^{PLA}$  is the percentage of PLA in the polymeric nanostructured mats.

### 2.5.5. Nanofibers' mechanical aspects

PLA/PEG and PLA/PEG/OPN (12.5, 25, and 50 % w/w) nanofiber membranes' rectangular specimens (3.2 × 0.7 mm) were conditioned at 25 °C and 50 % RH for a minimum of 48 h and subjected traction testing using a dynamic-mechanical thermal analyzer (DMA Q800 model, TA Instruments, Inc.) equipped with an 18 N load cell. The nanofibers were stretched at 0.1 %.min<sup>-1</sup>. Each sample was tested with at least 10 specimens. The mechanical properties, including elastic modulus (EM), were determined from the linear slope of the stress versus strains curves. The tensile strength (TM) was calculated by dividing the maximum force by the initial cross-sectional area. Elongation at break ( $\epsilon$ ) was calculated using Eq. 2, where  $d$  represents the final displacement, and  $d_0$  is the initial clamp-to-clamp distance:

$$\epsilon(\%) = \frac{d - d_0}{d_0} \times 100 \quad (2)$$

From values obtained in the stress versus strain graphs, films' toughness was calculated from the area below the curve.

### 2.5.6. Swelling properties (Ws)

The nanofibers membranes' water absorption capacity (Ws) was evaluated following the methods outlined by Fahimirad et al. [68]. Initially, the PLA/PEG and PLA/PEG/OPN (12.5, 25 and 50 % w/w) nanofiber membrane samples were weighed ( $W_d$ ). Subsequently, these samples were immersed in the PBS solutions for 72 h. After that period, the nanofiber samples were extracted, excess water on the nanofibers was removed using a filter paper, and the samples were reweighed ( $W_w$ ). The water adsorption capacity (Ws) was calculated according to Eq.3:

$$Ws(\%) = \frac{W_w - W_d}{W_d} \times 100 \quad (3)$$

### 2.5.7. Water vapor permeability rate (WVPR)

The nanofibers' water barrier properties were determined using the modified ASTM method E96/16 [69]. The samples were cut into circles (approximately 20 mm) and sealed on the top of permeation cells containing dried silica gel to provide constant relative humidity (RH). Subsequently, the cells were stored in a desiccator containing distilled water (100 %RH;  $2.337 \times 10^3$  Pa, vapor pressure at 20 °C). The water vapor's gravimetric quantification transferred through the nanofibers was conducted for 18 h. This analysis period was determined based on the necessary dressing changes and the study by Al-Naymi et al. [70] and Zhong et al. [71]. Water vapor permeability (WVP) (g.mm.kPa<sup>-1</sup>.h<sup>-1</sup>.m<sup>-2</sup>) was calculated using Eq. 4:

$$WVP = \frac{W \cdot \delta}{A \cdot t \cdot \Delta P} \quad (4)$$

where  $W$  is the change in cell weight [g],  $\delta$  is average film thickness [m], and  $A$ ,  $t$ , and  $\Delta P$  are exposed film area [m<sup>2</sup>], time [s], and partial water vapor pressure differential [Pa], respectively. The average WVP value for each sample was obtained in triplicate.

### 2.5.8. Water contact angle measurement

The nanofibers' water contact angle was assessed to determine their hydrophilicity using a Theta Lite optical tensiometer (dpUnion, Jabaquara, Brazil). Six drops of distilled water (2  $\mu$ L) were randomly placed on the surface of each nanofiber sample at room temperature. Images and contact angles were obtained using OneAttension software (dpUnion, Jabaquara, Brazil). The water contact angle values for PLA/PEG and PLA/PEG/OPN (12.5, 25 and 50 % w/w) nanofibers were expressed as the average value (AV)  $\pm$  standard deviation (SD). The contact angle tests were carried out following the studies by Habibi et al. [72], Zhang et al. [73], Ding et al. [74], Sharifi et al. [6] and Tri et al. [75].

### 2.5.9. Antioxidant activity study

The assay was carried out according to the methodology reported by da Silva Uebel et al. [76]. The OPN, PLA/PEG and PLA/PEG/OPN (12.5, 25, and 50 % w/w) nanofiber samples were analyzed for radical scavenging activity against the 2,2-diphenyl-1-picrylhydrazyl (DPPH) radical, which were read using a UV-Vis spectrophotometer. For bioactive compounds extraction from the nanofibers (12 % PLA/PEG, 12 % PLA/PEG/OPN 12.5 %, 25 %, and 50 % w/w solutions), 1 mL chloroform and 2 mL ethanol were added to 1 g of each nanofibers sample. These dispersions were placed in an ultrasonic bath (Sinergia Científica, Campinas-SP, Brazil) for about 3 h. Afterward, 8 mL methanol was added to the nanofibers PLA/PEG and PLA/PEG/OPN (12.5, 25, and 50 % w/w). The samples were again placed in an ultrasonic bath for 10 min and centrifuged using a Hettich Universal 320 centrifuge (Analítica, São Paulo-SP, Brazil) for approximately 5 min at 4000 rpm.

The DPPH solution was prepared on the analysis day at a 6.0 mg/250 mL methanol concentration. For assay performance, 2 mL of the DPPH solution were added to 2 mL of the bioactive compound sample extracted from the nanofibers. In addition, a control solution (chloroform, ethanol, and methanol) was prepared using 2 mL of the mixture of nanofibers solvents solution without bioactive compounds and 2 mL DPPH solution. The samples were maintained in the dark at room temperature. After 30-min incubation at room temperature in the dark, the solution's absorbance was recorded at 517 nm using a UV-Vis Spectrometer (Shimadzu 1600). The free radical scavenging efficiency was calculated by Eq. 5:

$$\text{Radical scavenging activity (\%)} = \frac{\text{Control}_{OD} - \text{Sample}_{OD}}{\text{Control}_{OD}} \times 100 \quad (5)$$

where Control<sub>OD</sub> is the absorbance of the aqueous control DPPH (DPPH and solvents), and Sample<sub>OD</sub> is the absorbance of the aqueous DPPH solution and bioactive compound sample extracted from the nanofibers.

### 2.5.10. Cell cytotoxicity evaluation

For the test, murine fibroblasts derived from connective tissue (L929) acquired from the ATCC (American Type Culture Collection), provided by the Araraquara Campus/ São Paulo State University (UNESP) Dentistry laboratory, were used. Initially, the cells were cultured in Dulbecco's Modified Eagle's Medium (DMEM) supplemented with 10 % Fetal Bovine Serum (FBS) and antibiotics (penicillin 100 U/mL; streptomycin 0.1 mg/mL) and then oven incubated at 37 °C and 5 % CO<sub>2</sub>. After 2 consecutive rings, the cytotoxicity test was started using a  $1 \times 10^4$  cells/well concentration, which was incubated in a 96-well plate. The plate was kept in an incubator for 24 h, using the same temperature and CO<sub>2</sub> percentage parameters described above. At the same time as the cells were plated, the extraction media (treatment) using PLA/PEG and PLA/PEG/OPN-25 % polymer fibers were prepared following ISO 10993-12.<sup>57</sup> To this end, 4 cm<sup>2</sup> of each film was placed in a microtube with a 2 mL culture medium addition (DMEM +10 % fetal bovine serum). The nanofibers in contact with the media were left to stir for 24 h at 37 °C. After that, the stirring period was over, the media was filtered through a 0.22  $\mu$ m syringe filter. After filtering, they were added to the

cell monolayer using 100  $\mu\text{L}$ /well and incubated in a  $\text{CO}_2$  oven for 48 h. Afterward, the extraction media was removed and washed twice with Phosphate Buffered Saline (PBS). After that, 100  $\mu\text{L}$  of MTT (3-(4,5-Dimethylthiazol-2-yl)-2,5-Diphenyltetrazolium Bromide) previously diluted to a 1 mg/mL concentrations were added to each well. The plate was incubated again at 37  $^\circ\text{C}$  and kept in the dark until violet formazan crystals formation was observed (3 h). At the end of the incubation period, the MTT was removed from the wells, and the formed crystals were dissolved by adding 50  $\mu\text{L}$  absolute isopropyl alcohol. The absorbance values (Abs) were obtained on a microplate spectrophotometer (SoftMax<sup>®</sup> Pro 5) with a 570 nm wavelength reading. As a cell death control (positive control), the cells were treated with 10 % DMSO (Dimethylsulfoxide), and as a survival control (negative control), the cells were treated with DMEM +10 % SFB. The experiments were conducted in triplicate, in three independent trials, including the controls. With the Abs values, the average percentage of cell viability was calculated in relation to the survival control (100 %), as shown in Eq.6 (ISO standard 10993-5) [77]:

$$\frac{(\text{Sample Abs} - \text{White Abs})}{(\text{Survival control Abs} - \text{White Abs})} \times 100 \quad (6)$$

### 2.5.11. Cell proliferation and adhesion test

For the cell adhesion test, the cells were seeded at a  $2 \times 10^5$  cells density on the materials to be tested for 48–72 h in an oven at 37  $^\circ\text{C}$  under a 5 %  $\text{CO}_2$  humidified atmosphere. The culture medium was then aspirated, and the matrices were washed with DPBS buffer and fixed in 4 % paraformaldehyde for 15 min. The matrices were rewashed with DPBS, and then DAPI (5 mg/mL) was added and incubated at room temperature for 5 min, followed by dehydration with a gradient ethanol concentration (30, 50, 75, 85, 90, 95 and 100 %) for 15 min, respectively. SEM was used to determine adhesion on the materials' surface.

## 2.6. Statistical analysis

The results were submitted to analysis of variance (ANOVA) and Tukey's multiple comparison test, both at a 5 % significance level ( $p < 0.05$ ) using the Sisvar<sup>®</sup> (Version 5.4) statistical software.

## 3. Results and discussions

### 3.1. OPN chemical composition

OPN was composed, on a dry basis, of  $41.0 \pm 1.0$  % carbohydrates,  $20.8 \pm 0.2$  % protein,  $14.0 \pm 2.0$  % ash,  $3.1 \pm 0.1$  % lipids and  $22.0 \pm 0.3$  % total fiber. Martin [52] used mucilage from OPN and found a carbohydrate and protein composition of 48 % and 19 % w/w,

respectively, which corroborates the values found in this study. However, Oliveira [78] and Lima Júnior [79] found a  $79.93 \pm 0.29$  % carbohydrate and  $8.89 \pm 0.17$  % protein, 46.88 % carbohydrate and 10.47 % protein composition, respectively. Such differences are due to changes in the process of obtaining the mucilage. OPN was also characterized by lignin, cellulose, and hemicellulose content, showing values of approximately  $11.3 \pm 0.1$  %,  $20.0 \pm 0.1$  % and  $21.0 \pm 0.1$  % respectively. According to these values, OPN presents characteristics of fibers derived from secondary cellulose sources, i.e., low cellulose concentration but relatively high hemicellulose concentration [80].

### 3.2. Rheological characterization

The rheological behavior of PLA/PEG spinning solutions with different OPN contents (12.5, 25, and 50 % w/w) is shown in Fig. 2A and B.

Overall, the polymer viscosity is linked to irreversible deformation through molecular chains sliding past adjacent chains [81]. The increase in OPN content (relative to PLA/PEG) led to higher viscosity values, increasing from 4.4 to 9.6 (12.5 % OPN), 12.1 (25 % OPN), and 12.1 (50 % OPN) mPa.s, respectively, as shown in Fig. 2A. This suggests a complex viscosity compared to the pure PLA/PEG solution, possibly related to more significant restriction of polymer mobility. In addition, the increase in viscosity values by incorporating OPN into the PLA/PEG solution is correlated with the dense entanglement between nanofibers, as confirmed by SEM images (Fig. 3A). Therefore, it is one of the reasons for the significant increase in nanofiber diameter (Fig. 3B). Notably, no thinning behavior was observed with increasing shear rate, resulting in higher viscosity and elevated storage moduli (Fig. 2B) with OPN incorporation. It may be asserted that no agglomeration occurred, thus not affecting OPN distribution in the nanofibers and interaction with the PLA/PEG matrix. The same was also observed in the studies by Jubinville et al. [81]. In terms of moduli, the addition of particles to a system increases the material's elasticity, causing the storage modulus ( $G'$ ) to increase, while the loss modulus ( $G''$ ) increases due to particle-particle interaction. Overall, all PLA/PEG and OPN incorporated solutions (12.5, 25 and 50 % w/w), the viscoelastic behavior was more similar to solid since  $G' > G''$ . This suggests, better network formed between the OPN particles and PLA/PEG due to the improved compatibility. These results align with those by Jubinville et al. [81].

### 3.3. Nanofibers morphology

The morphology of pure PLA/PEG nanofiber membranes containing different OPN concentrations (12.5, 25 % and 50 % w/w) was analyzed by SEM. Fig. 3A and B show the nanofiber membranes SEM images, the

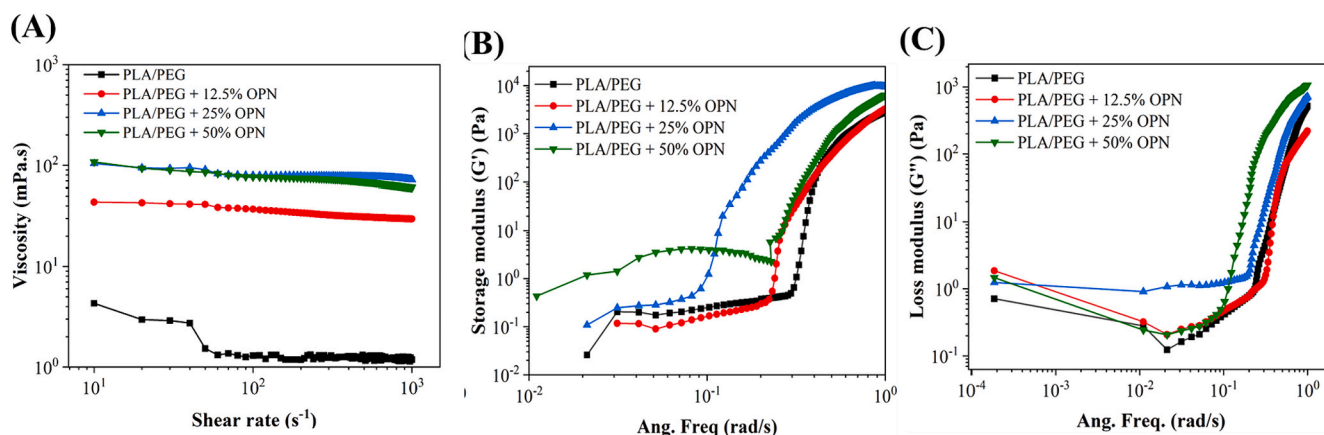
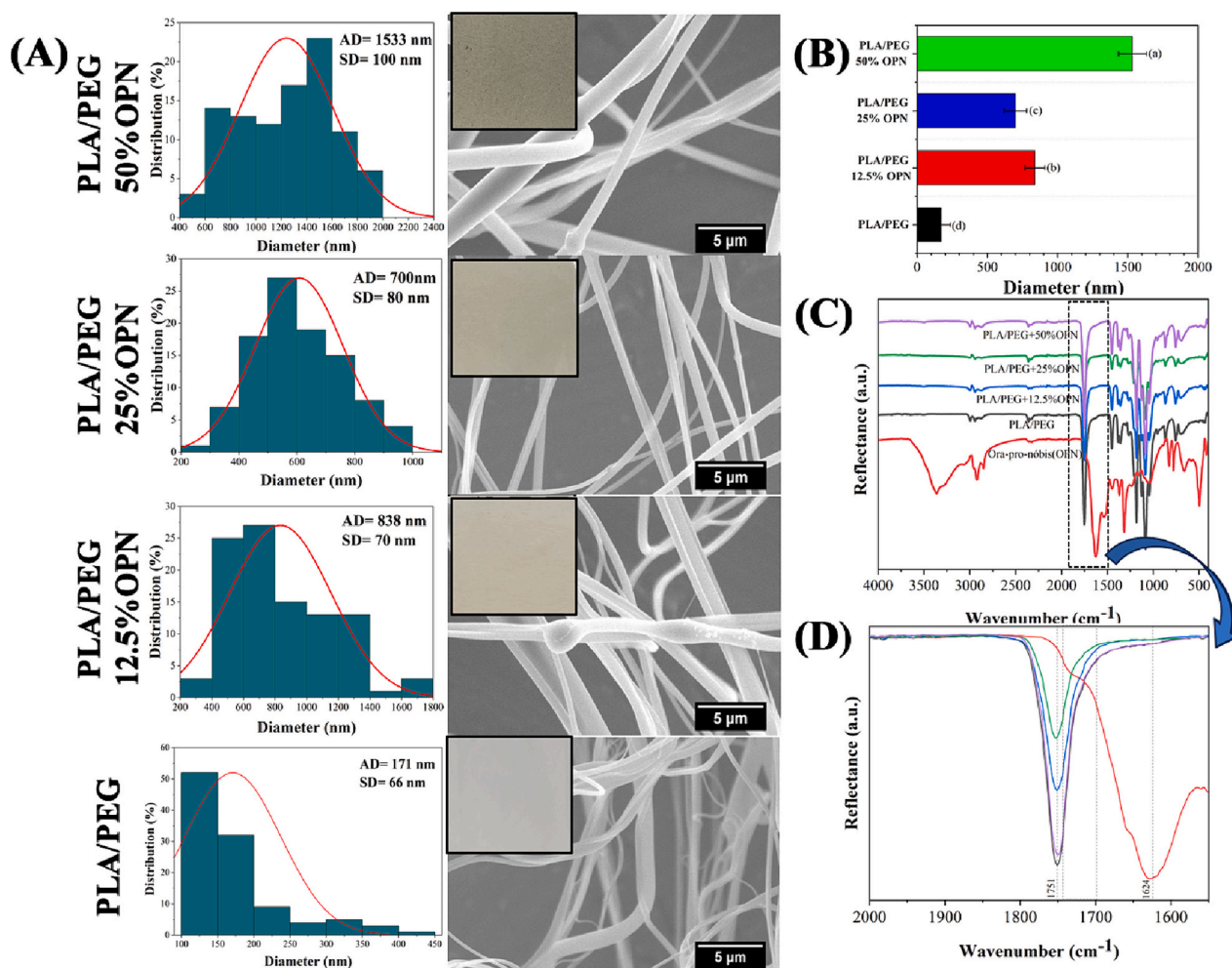


Fig. 2. (A) Viscosity and (B) Storage modulus (C) Poly(lactic acid) (PLA)/ poly(ethylene glycol) (PEG) SBS fibers loss modulus influenced by varying Ora-pro-nóbis concentrations (OPN; 12.5, 25, and 50 % w/w).



**Fig. 3.** SBS characterization comprising poly(lactic acid) (PLA)/ poly(ethylene glycol) (PEG) as influenced by different Ora-pro-nóbis (OPN) concentrations (OPN; 12.5, 25 and 50 % w/w) fibers morphology and size (A) Representative scanning electron microscopy (SEM) (right panels) and nanofiber membranes images. Scale bar: 5  $\mu$ m. Fibers' size (diameter) distribution ( $n = 80$ ) was calculated from SEM micrographs (left panels). Red lines indicated fitted Gaussian distributions. (B) SBS fibers' average diameter. (C) Attenuated total reflectance Fourier-transform infrared spectra (ATR-FTIR) of PLA/PEG and PLA/PEG/OPN (12.5, 25 and 50 % w/w)'s SBS fibers. (D) Expanded ATR-FTIR.

diameter distribution and the average diameter, respectively. Fig. 3A shows PLA/PEG and PLA/PEG/OPN (12.5, 25 %, and 50 % w/w) nanofiber membranes images.

As shown in Fig. 3A, the nanofibers' surface regular, bead-free, uniform, smooth surface, and randomly oriented fibers were found. This randomly oriented nanostructure morphology with no fiber interconnecting and branching prepares suitable conditions for gas or water vapor exchange and ensures a wet environment for wound healing with no scarring [8]. Furthermore, a relatively smooth surface, without OPN crystals on the surface, was found in all formulations, representing a complete drug fusion into the polymeric matrix with the SBS process. An interweaving of nanofibers incorporated with OPN (PLA/PEG/OPN) was observed (Fig. 3A), along the spinning working distance. The average diameters were 171, 838, 700 and 1533 nm at 0 %, 12.5 %, 25 % and 50 % w/w OPN concentrations (Fig. 3B), respectively. As previously suggested, the SBS solutions' physicochemical characteristics, mainly including viscosity (Fig. 2A), may remarkably influence the nanofibers' morphology and average size. Furthermore, it was observed that the nanofiber diameter is positively correlated with the viscosity. It suggests that the OPN extract was incorporated into the PLA/PEG matrix, with a consequent increase in its diameter due to the increase in solution viscosity (Figs. 2 and 3B). According to Dadol et al. [82] viscosity is closely related to the solution concentration, having a

pronounced effect on fibers in terms of fiber morphology and diameter. The increased viscosity of higher concentration solutions, as seen with incorporating OPN, possibly creates higher viscoelastic forces that resist axial stretching during spinning, resulting in a larger fiber diameter. Such concentration/viscosity effects are in line with reports in the literature [82,83]. Furthermore, as no granule formation was observed, especially in the PLA/PEG/OPN 25 % and PLA/PEG/OPN 50 % formulations, the OPN extract was uniformly dispersed inside the fibers. These results align with those of Klan et al. [84] and Alippilakkotte et al. [85]. Although they studied different materials to obtain the nanofibers, both studies observed a significant increase in the nanofibers diameter by incorporating respectively nanoparticles and extracts into the PVA and PLA matrix.

Fig. 4 shows the PLA/PEG and PLA/PEG/OPN nanofibers (12.5, 25, and 50 % w/w) EDS mapping. It was noted that the PLA/PEG sample used in this experiment is primarily composed of: carbon (C) and oxygen (O) [34]. Carbon is the predominant component, as PLA is a polymer linked by carbon-carbon bonds. Following OPN incorporation, the presence of other elements attributed to OPN composition became evident, as illustrated in Fig. 4 B-D. The PLA/PEG/OPN nanofibers (12.5, 25, and 50 % w/w) also presented a significant presence of C and O, similar to the results observed for PLA/PEG (Fig. 4A). The analysis further revealed the presence of calcium (Ca), potassium (K),

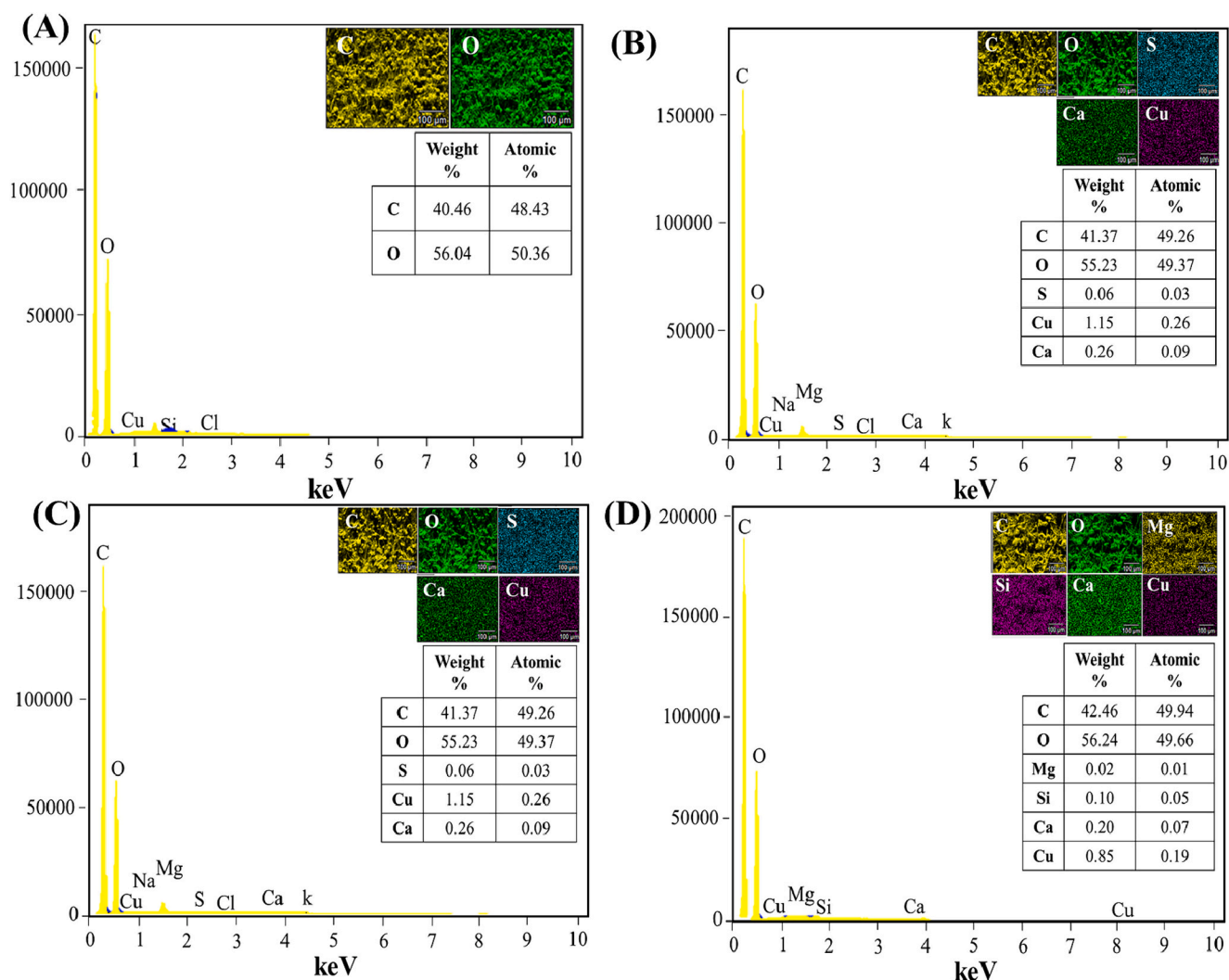


**Fig. 4.** Weight and atomic percentages, elemental color composition atoms together and separately of (A) poly(lactic acid)/poly(ethylene glycol) (PLA/PEG), (B) poly(lactic acid)/poly(ethylene glycol)/Ora-pro-nóbis 12,5 % w/w (PLA/PEG/OPN 12,5 %), (C) poly(lactic acid)/poly(ethylene glycol)/Ora-pro-nóbis 25 % w/w (PLA/PEG/OPN 25 %) and (D) poly(lactic acid)/poly(ethylene glycol)/Ora-pro-nóbis 50 % w/w (PLA/PEG/OPN 50 %).

magnesium (Mg), and chlorine (Cl), which are in line with OPN's chemical composition, as indicated in Section 3.1. Similar results were observed in previous studies conducted by Oliveira et al. [86]. Furthermore, OPN incorporation into the nanofibers was confirmed and they were uniformly distributed.

### 3.3.1. Fourier transform infrared spectroscopy (FTIR)

The ATR-FTIR spectra shown in Fig. 3C were carried out to check for possible PLA/PEG and OPN interactions. The OPN spectrum (Fig. 3C) showed bands specific to materials containing proteins and carbohydrates, which is in agreement with the studies by Tan et al. [87], Andrade et al. [88], Neves et al. [57], and Conceição et al. [89]. Bands at  $3363\text{ cm}^{-1}$  (stretching vibrations -OH),  $2923$  and  $2853\text{ cm}^{-1}$  (aliphatic carbons -CH(CH<sub>2</sub>) and -CH(CH<sub>3</sub>)),  $1623\text{ cm}^{-1}$  (amide I),  $1373\text{ cm}^{-1}$  (-COO-),  $1226\text{ cm}^{-1}$  (stretching vibrations -CC) and  $668\text{ cm}^{-1}$  (bending deformation -CH) were observed. Also, the bands at  $1372$  and  $1052\text{ cm}^{-1}$  were attributed to amide III (-CN stretching) of oligopeptides covalent bonds [87] and the -CO stretching vibrations of alcohols, respectively. [88] The band at  $832\text{ cm}^{-1}$  is attributed to the -CH ring out-of-plane bending [90]. All PLA/PEG nanofiber membranes absorption bands are characteristic of PLA and PEG functional groups, observed around ca.  $2994$ ,  $2936$ ,  $2870$ ,  $1752$ ,  $1449$ ,  $1370$  and  $1077\text{ cm}^{-1}$ . The PLA/PEG showed characteristic stretching frequencies for -CH<sub>3</sub>

asymmetric ( $2994\text{ cm}^{-1}$ ), -CH<sub>3</sub> symmetric ( $2936\text{ cm}^{-1}$ ), and -CO single bond stretching vibration ( $1195\text{ cm}^{-1}$ ). It also presented bending frequencies for -CH<sub>3</sub> asymmetric ( $1449\text{ cm}^{-1}$ ) and -CH<sub>3</sub> symmetric ( $1370\text{ cm}^{-1}$ ) [1,3,15].

For the ATR-FTIR spectra of PLA/PEG/OPN nanofibers (12.5 %, 25 %, and 50 % w/w), although no significant changes were identified in the spectra due to PLA/PEG and OPN bands overlap, such limitation may be attributed to the challenges of incorporating a hydrophilic component (OPN) into a hydrophobic matrix (PLA/PEG), as well as the components' complete encapsulation, corroborating with the studies by Brunet et al. [91]. Possible interactions were observed by expanding the  $2000$  to  $1500\text{ cm}^{-1}$  region (Fig. 3D, expanded). It suggested that secondary interactions may have occurred between OPN and PEG. Specifically, the incorporation of OPN caused a slight reduction in the  $1751\text{ cm}^{-1}$  band (-CO) (Fig. 3D, expanded). It may aim to form hydrogen bonds with water and, consequently, lead to increased hydrophilicity. This is vital role in determining the WVTR (Fig. 7B) and the contact angle between water and the material. It therefore, plays a crucial role in improving the biomaterial's ability to be used as a dressing material. In addition, PLA/PEG/OPN nanofibers showed a subtle band at  $1722\text{ cm}^{-1}$ , corresponding to the -COO functional group. Such a band is characteristic of a carboxylic group presence in the OPN leaf mucilage, which may serve as a site for ionic bonds, contributing to the gel-forming capacity.

This is consistent with the studies of Pinto et al. [51], Behnaz et al. [51] and Neves et al. [57]. Therefore, the FTIR analysis validated the successful OPN incorporation into the nanostructured membranes (Fig. 3C and D).

### 3.4. Thermal properties

The thermal stabilities of nanofiber membranes added or not with OPN (12.5, 25, and 50 % w/w) and their respective pure constituents were evaluated by DSC and TG/DTG, which are shown in Fig. 5A and B, respectively. The temperatures corresponding to the onset (Td,onset) and offset (Td,offset) of thermal degradation, glass transition temperature (Tg), crystallization temperature (Tc), melting temperature (Tm), melting enthalpy ( $\Delta H_m$ ), and crystallization enthalpy ( $\Delta H_c$ ) are presented in Table 1. Notably, all the nanofiber membranes showed no mass loss up to 100 °C, indicating no perceptible residual solvent in the nanofibers produced. It was in line with the studies by Mendes et al. [66].

Overall, PLA/PEG and PLA/PEG/OPN nanofiber membranes showed two mass loss phases, while the OPN sample showed three phases, as seen in Fig. 5B. In the OPN sample, the first mass loss was observed at around 99 °C (3 %) due to the water content [78]. The mass loss between (Td,onset) 202 and (Td,offset) 462 °C (~57 %, DTG: 301 °C) corresponded to the main components' chemical decomposition in its composition (Section 3.1), such as polysaccharides and proteins. After degradation at 600 °C (Fig. 5B) a 14 % residue was observed due to OPN's high carbon and mineral content. Similar results were observed in the studies by Conceição et al. [89] and Mercê et al. [92].

The PLA/PEG and PLA/PEG/OPN nanofiber membranes (12.5 %, 25 % and 50 % w/w) showed the first mass loss phase at approximately (Td,onset) 270–311 °C (~88 %, 92 %, 93 % and 98 %, respectively) and DTG from 333 to 351 °C, which was due to the polymer's main chains rupture, and intra- and inter-molecular transesterification reactions [5]. It is well known that the biodegradable polyesters (PLA)'s thermal decomposition a competition between random chain scission by cis-elimination (generating an acrylic ester unit) and cyclic rupture by intramolecular transesterification (releasing lactic acid) [93]. OPN incorporation

increased the PLA/PEG initial temperature, thus improving its stability. For the PLA/PEG/OPN12.5 %, PLA/PEG/OPN25%, and PLA/PEG/OPN50% mats, a mass loss was observed starting at (DTG) 324, 334, and 351 °C, respectively (Table 1). Above 300 °C, the OPN-incorporated nanofibers exhibited improved thermal stability due to OPN's low degradation rate, corresponding to the peak lower intensity and the shift of the peak position to a higher temperature in the DTG curves (Fig. 5B). Increased thermal stability for PLA/PEG nanofibers suggests that OPN incorporation may have increased the molecular interactions between adjacent PLA/PEG chains, as well as reinforcing the potential interactions with the ester group of PLA and the apolar compounds found in the OPN composition, as indicated by the FTIR (Fig. 3C) and DSC (Fig. 5A). Also, according to Table 1, it was observed that the onset degradation temperature (Td,onset) of OPN was higher than that of PLA/PEG, indicating greater thermal stability. This may be associated with the OPN's composition (Section 3.1), and the complete OPN dispersion in the PLA/PEG matrix, as verified by the nanostructures' morphology (Fig. 3A).

The DSC analysis investigated the nanofibers thermal behavior. According to the DSC curves, the crystallinity indexes (CI) of PLA/PEG and PLA/PEG/OPN at 12.5 %, 25 %, and 50 % w/w were calculated, resulting in values of 35 %, 45 %, 75 %, and 43 %, respectively. It indicated that the CI of PLA/PEG nanofibers loaded with OPN was higher than that of pure PLA/PEG fiber mat. Crystallization of PLA/PEG incorporated with OPN is easier due to increased chain mobility at lower temperatures, which was attributed to the increased free volume between the PLA/PEG chains. DSC measurements revealed two PLA/PEG endothermic peaks at 40 °C and 170 °C ( $\Delta H_m = 43$  J/g), corresponding to Tg and Tm, respectively, in line with the temperature range reported in the literature [15]. The exothermic peaks (cold crystallization temperature (Tc)) of PLA/PEG appeared close to 73 °C.

Incorporating OPN at 12.5, 25 and 50 % w/w concentrations did not significantly alter the Tm of PLA/PEG, remaining relatively constant at 170 °C. However, the Tg values of PLA/PEG/OPN nanofiber mats increased by approximately ~25 % (12.5 % OPN), ~30 % (25 % OPN), and ~35 % (50 % OPN), respectively, due to the presence of charges, which limited the PLA/PEG chain mobility (Table 1). Furthermore, the

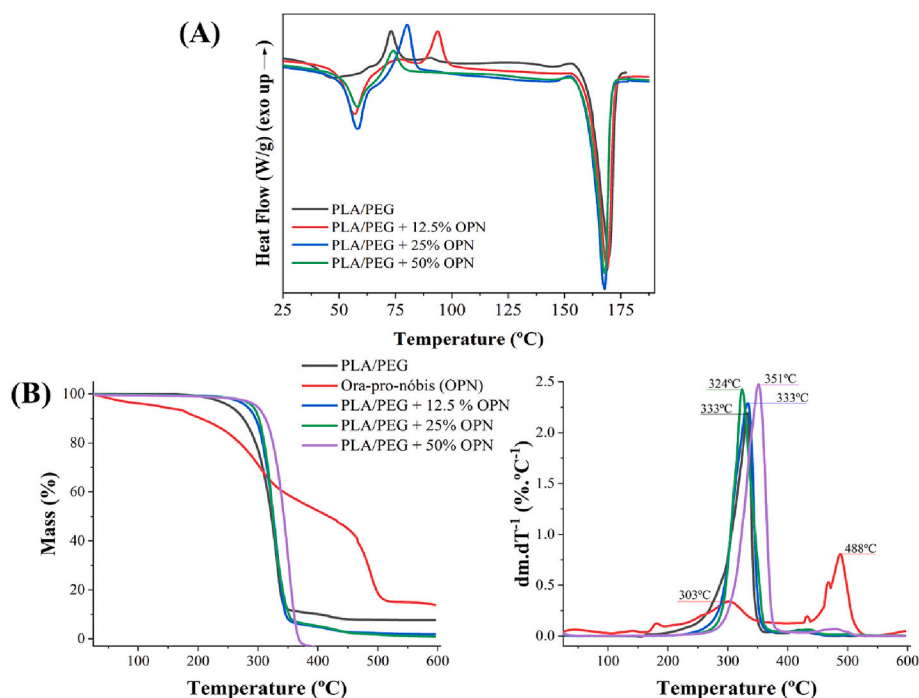


Fig. 5. (A) Differential scanning calorimetric thermograms (DSC). (B) Thermogravimetric (TG; left) and derivative TG (right) profiles of poly(lactic acid) (PLA) poly(ethylene glycol) (PEG) SBS fibers influenced by varying Ora-pro-nóbis concentrations (OPN; 12.5, 25 and 50 % w/w).

**Table 1**

Thermal parameters – initial (Td,onset) and final (Td,offset) degradation temperatures, derivative Thermogravimetry (DTG), (glass transition temperature (Tg), crystallization temperature (Tc), melting temperature (Tm), melting enthalpy ( $\Delta H_m$ ), crystallization enthalpy ( $\Delta H_c$ ), and crystallinity index (CI) of nanofibers comprising poly (lactic acid) (PLA)/ poly(ethylene glycol) (PEG) as influenced by different Ora-pro-nóbis (OPN) concentrations (OPN; 12.5, 25 and 50 % w/w).

Sample	Td,onset (°C)	DTG (°C)	Td,offset (°C)	Tg (°C)	Tc (°C)	Tm (°C)	$\Delta H_m$ (J/g)	$\Delta H_c$ (J/g)	CI (%)
Ora-pro-Nobis (OPN) OPN in fibers (%) <sup>*</sup>	202	301	467	–	–	–	–	–	–
0	278	333	341	40	73	170	43	10	35
12.5	293	324	343	50	94	169	43	6	45
25	298	334	351	52	80	168	45	15	75
50	311	351	368	54	74	168	41	6	43

Values with different letters in the same column were significantly different ( $p \leq 0.05$ ).

<sup>\*</sup> OPN: Ora-pro-nóbis concentration in the blow-spinning fibers solution (w/w, dry mass).

OPN molecules into the PLA/PEG macromolecules increased the crystallization rate, shifting Tc to lower values and increasing the degree of crystallinity (Table 1). By incorporating OPN at 25 and 50 % w/w, the cold crystallization peak became broader and shifted to lower temperatures compared to pure PLA/PEG. The lower Tc values observed may indicate faster cold crystallization induced by OPN incorporation, which acts as nucleating agents for PLA/PEG. For PLA/PEG/OPN 12.5 %, the Tc peak shifted to higher values than in pure PLA/PEG. For us, this behavior resulted from a possible better adhesion to the matrix due to the lower added load, allowing for a better interaction with PEG and PLA. This could hinder the crystallization process by reducing nucleation sites, leading to higher Tc values, corroborating with the studies by Frone et al. [94].

It is important to note that the PLA/PEG nanofiber mats, with or without OPN, remained well below their initial degradation temperatures and associated thermal events. As a result, they are not affected by any temperature changes that may occur during the use, transportation, or storage of controlled-release devices.

### 3.5. Nanofiber membranes' mechanical properties

Nanofiber membranes used for wound dressings must have good mechanical properties, so the stress-strain behavior of PLA/PEG-based nanofiber membranes incorporated or not with OPN (12.5, 25 and 50

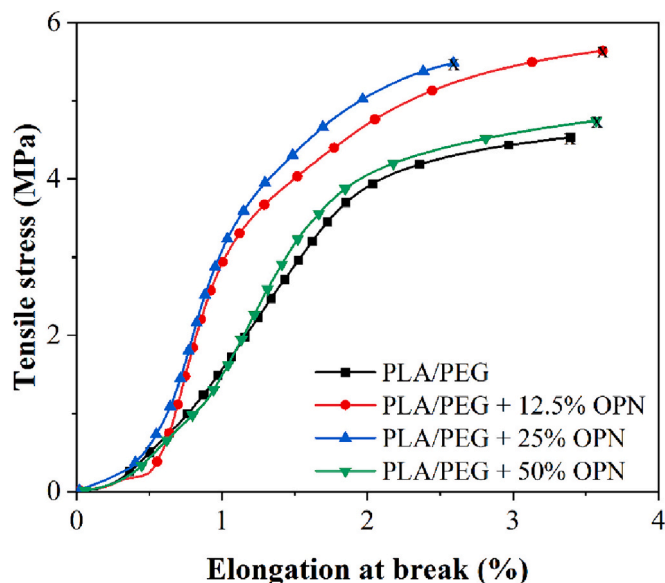


**Fig. 6.** Stress-strain curves of poly(lactic acid) (PLA)/poly(ethylene glycol) (PEG) SBS fibers influenced by varying concentrations of Ora-pro-nóbis (OPN; 12.5, 25 and 50 % w/w). The X in the stress versus strain curve indicates rupture.

% w/w) was analyzed, and the results are shown in Fig. 6 and Table 2. The among OPN and PLA/PEG interactions was significant ( $p < 0.05$ ) for the elastic modulus (EM), tensile strength (TS), elongation at break ( $\epsilon$ ), and toughness (T).

PLA/PEG nanofiber membranes exhibited a 3.4 MPa TS with a 3.5 %  $\epsilon$  (%) and 14 MPa EM. A similar result was observed by Alharbi et al. [27], who showed a weak and fragile mechanical response. Notably, the incorporation of OPN into PLA/PEG-based nanofibers allowed for a significant increase in mechanical properties compared to PLA/PEG, especially with a TS increase of around 65 % (PLA/PEG/OPN 12.5 %), 59 % (PLA/PEG/OPN 25 %) and 26 % (PLA/PEG/OPN 50 %), respectively. Similar behavior was observed in EM values, increasing significantly ( $p < 0.05$ ) of 464 % (PLA/PEG/OPN 12.5 %), 336 % (PLA/PEG/OPN 25 %) and 43 % (PLA/PEG/OPN 50 %), indicating that OPN acts as a reinforcing filler. This is attributed to the stiffening occurrence by OPN dispersion in the PLA/PEG. However, there was a slight reduction in the TS and EM values of PLA/PEG/OPN50% nanofibers, which may be associated with a possible aggregation of the filler within the nanofibers (although not observed in the SEM images, Fig. 3A), leading to stress points. It indicates that low filler reinforcement concentrations enhanced the mechanical properties. At the same time, the aggregations provided at high filler concentrations may weaken their mechanical performance, creating structures resembling defects in the fibers. A similar result was observed in the studies by Karbowniczek et al. [95].

The polymeric nanofibers' mechanical properties depend on many factors including their structure, and the interactions between each of the polymer components in scaffolds. For example, the DSC patterns (Fig. 5A), indicated greater crystallinity (Table 2) when OPN was added. These characteristics are in line with more mechanically resistant and tougher nanofibers. Additionally, PLA/PEG and OPN components interactions, as suggested by FTIR (Fig. 3C and D), may also occur, and contributing to increased crystallinity (Table 2) and, consequently,

**Table 2**

Mechanical properties – Thickness ( $\epsilon$ ), Tensile strength (TS), Elongation at break ( $\epsilon\%$ ) Elastic modulus (EM), and Toughness (T) –of nanofibers comprising poly (lactic acid) (PLA)/poly(ethylene glycol) (PEG) as influenced by different Ora-pro-nóbis (OPN) concentrations (OPN; 12.5, 25 and 50 % w/w).

Samples OPN in fibers (%)	Thickness ( $\epsilon$ ) ( $\mu\text{m}$ )	TS (MPa)	$\epsilon\%$ (%)	EM (MPa)	T (MPa)
0	0.13 $\pm$ 0.04 <sup>a</sup>	3.40 $\pm$ 0.05 <sup>b</sup>	3.50 $\pm$ 0.20 <sup>a</sup>	14.0 $\pm$ 3.2 <sup>b</sup>	2.5 $\pm$ 0.6 <sup>a</sup>
12.5	0.15 $\pm$ 0.03 <sup>a</sup>	3.80 $\pm$ 0.50 <sup>b</sup>	3.50 $\pm$ 0.20 <sup>a</sup>	79.0 $\pm$ 10.0 <sup>a</sup>	8.0 $\pm$ 0.8 <sup>a</sup>
25	0.14 $\pm$ 0.04 <sup>a</sup>	5.30 $\pm$ 0.20 <sup>a</sup>	2.80 $\pm$ 0.13 <sup>b</sup>	61.0 $\pm$ 14.0 <sup>a</sup>	10.0 $\pm$ 0.2 <sup>a</sup>
50	0.17 $\pm$ 0.03 <sup>a</sup>	4.10 $\pm$ 0.70 <sup>ab</sup>	3.50 $\pm$ 0.34 <sup>a</sup>	20.0 $\pm$ 1.8 <sup>b/</sup>	6.2 $\pm$ 0.5 <sup>a</sup>

Mechanical attributes were reported as average values and standard deviations. The same letters on the same column indicate that the values were not statistically significant ( $p > 0.05$ ) using Tukey's test.

strength. According to the studies by Mohammadi et al. [29], the increase in mechanical properties is attributed to the nanofibers' structure and the interactions between the components found in them. The nanofibers' diameter may have influenced these properties, as nanofibers typically exhibit size-dependent behavior, wherein the fibers' ductility increases as their diameter increases. This phenomenon explained the observed increase in strength (TS) and toughness (T) in OPN-embedded nanofiber membranes (Table 2). These theories are supported by Hassim et al. [96] and Mohammadi et al. [29]. Moreover, other factors may have influenced the mechanical properties of the nanofiber membranes added or not with OPN, such as the length, alignment, and entanglement of the fibers within the membranes, as seen in the SEM images (Fig. 3A) [27,97].

On the other hand, the results in Fig. 6 and Table 2 showed that the deformation at break did not change with the incorporation of OPN at 12.5 and 50 % w/w concentrations. However, it resulted in a 20 % reduction in PLA/PEG/OPN 25 % nanofibers. Although the exact mechanism remains unclear, several factors may contribute concomitantly or separately to this observation. The OPN may have acted as a potential plasticizer, given its composition (Section 3.1), which has high carbohydrate content. It may be related to an excess of hydrocolloids leading to the formation of non-associated regions, allowing flexibility in the polymeric chains. Additionally, incorporating of OPN increased the fiber diameter (Fig. 3B), consequently reducing the specific surface area. These factors may lead to a friction resistance reduction between the fibers and a decrease in relative sliding and  $\epsilon\%$  of the nanofiber membranes. These results were supported by Perez-Puyana et al. [98] and Zhu et al. [99]. Regardless of the mechanism, the nanofibers exhibited TS and  $\epsilon\%$  values close to the tensile strength (TS: 1 to 32 MPa) and elongation ( $\epsilon\%$ : 0.42–2.26 %) of human skin [68,100]. Therefore, the developed PLA/PEG/OPN composite membranes are a potential

candidate for wound dressing applications.

### 3.6. Wettability, barrier, and swelling properties

Nanofiber membranes must exhibit essential properties to establish their effectiveness as dressing materials. Additionally, wettability, water vapor transmission rate (WVTR), and swelling behavior properties, shown in Fig. 7A-C, respectively, were investigated.

Nanofiber membranes' wettability was assessed through water contact angle measurements and is shown in Fig. 7A. PLA/PEG nanofibers exhibited a contact angle ( $\theta$ ) of  $117^\circ$  (Fig. 7A), indicating a hydrophobic character, consistent with findings in other studies [34]. Similar behavior was observed in the OPN-incorporated nanofiber membranes (12.5, 25, and 50 % w/w) despite a significant ( $p < 0.05$ ) reduction in the contact angle. It suggests that as the OPN concentration increased and due to its hydrophilic nature (Fig. 3C), with an intense -OH band, polar groups were incorporated, leading to a decreased in the PLA/PEG nanofiber membranes's hydrophobicity. This supports OPN encapsulation inside the nanofibers, while the membrane surface primarily comprises PLA/PEG. Han et al. [33] found a similar result when incorporating cinnamaldehyde and tea polyphenol into PLA matrices, causing a slight reduction in nanofiber membranes' hydrophobicity. However, the contact angles of PLA/PEG and PLA/PEG/OPN nanofiber membranes (12.5, 25, and 50 % w/w) remained above  $90^\circ$ , indicating their overall hydrophobic nature. According to Zhao et al. [34] and Yin, J., Xu, L. and Ahmed, A. [101], such hydrophobicity in PLA/PEG and PLA/PEG/OPN nanofiber membranes may reduce dressing-wound adhesion, consequently reducing secondary injuries caused by dressing replacement or removal.

The wound healing process also depends on controlling the wound area's hydration, where an appropriate water vapor permeability rate

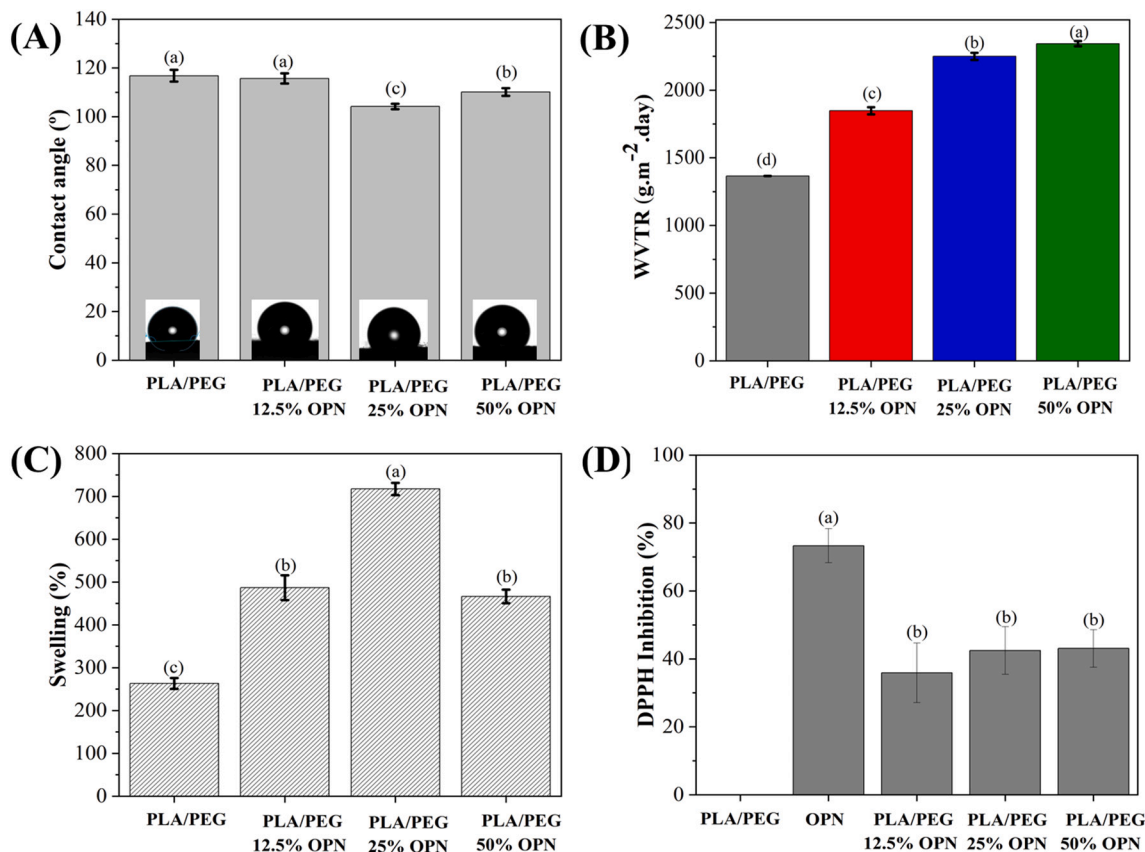


Fig. 7. (A) Water contact angles, (B) Water vapor permeability rate (WVTR), (C) Swelling properties, and (D) DPPH inhibition of nanofibers comprising poly(lactic acid) (PLA)/ poly(ethylene glycol) (PEG) as influenced by different Ora-pro-nóbis (OPN) concentrations (OPN; 12.5, 25 and 50 % w/w).

(WVTR) is an essential factor that facilitates moisture and gas exchange, thereby preventing the accumulation of wound exudate [68,102,103]. Thus, the WVTR properties of PLA/PEG nanofiber membranes incorporated with OPN (12.5, 25 and 50 % w/w) were analyzed and are shown in Fig. 7B. The PLA/PEG-based nanofiber membranes, incorporating different OPN concentrations, exhibited WVTR values ranging from 2343 to 1366 g/m<sup>2</sup>/day, as shown in Fig. 7B. It should be noted that an increase in the OPN concentration in the nanofibers significantly ( $p < 0.05$ ) enhanced WVTR. According to Ullah [32] the ideal WVTR range for a dressing to maintain adequate moisture at the wound site should be approximately 2000–2500 g.m<sup>-2</sup>.day<sup>-1</sup>, depending on the conditions and materials used. Human skin typically has a WVTR of  $204 \pm 12$  g.m<sup>-2</sup>.day<sup>-1</sup>, but for first-degree burns and granulation wounds, this value increases to  $279 \pm 26$  and  $5138 \pm 202$  g.m<sup>-2</sup>.day<sup>-1</sup>, respectively. For nanofiber membranes incorporated with OPN extract at 25 and 50 % w/w concentrations, the WVTR increased to 2250 and 2343 g.m<sup>-2</sup>.day<sup>-1</sup> (Fig. 7B), respectively, falling within the recommended range as ideal for wound closure dressings.

PLA/PEG and PLA/PEG/OPN nanofiber membranes (12.5, 25, and 50 % w/w) swelling properties were evaluated and are shown in Fig. 7C. The nanofiber membrane absorption capacity was assessed after 3 days of immersion. The swelling property is related to the materials' structural capacity to absorb local exudates at the wound site. It was observed that during the evaluated period, PLA/PEG nanofibers exhibited approximately 263 % swelling, while the swelling of OPN-incorporated nanofibers (PLA/PEG/OPN12.5 %, PLA/PEG/OPN25% and PLA/PEG/OPN50%) increased to 488 %, 717 %, and 466 %, respectively. According to Chen et al. [103], the greater swelling of nanofibers may be attributed to their increased hydrophilicity, supporting the findings of this study (Fig. 7A and B). It is important to note that all the nanofiber membranes maintained their structure without wrinkling or material loss. This enhanced swelling capacity and WVTR may assist with cell adhesion and migration, as observed in Fig. 8B. Therefore, these physicochemical properties of PLA/PEG nanofiber membranes, especially those containing OPN (PLA/PEG/OPN 12.5, 25 and 50 % w/w) exhibited desirable characteristics highly beneficial for the wound healing process.

### 3.7. Antioxidant activity study

Using nanofiber membranes incorporated with bioactive antioxidant compounds, such as OPN, may be beneficial for the wound healing

process, primarily by eliminating or reducing oxidative stress caused by the presence of free radicals and reactive oxygen species (ROS). This prevent damage to epithelial cells and the extracellular matrix (ECM), which could lead to a chronic issue [42]. The antioxidant activity of PLA/PEG and PLA/PEG/OPN nanofiber membranes (12.5, 25, and 50 % w/w) was determined using the DPPH radical scavenging method, and the results are shown in Fig. 7D. Due to the OPN composition's complexity, the antioxidant activity was related to the release tests, where the nanofiber mats' release profile when in contact with the liquid medium was verified, as reported by Jiang et al. [104]. As expected, the OPN extract exhibited high antioxidant activity against the DPPH radical (Fig. 7D), with approximately 73 % oxidation inhibition. This aligns with the studies by García et al. [2], Souza et al. [105], Hoff et al. [106], and Takeiti et al. [107], who showed that the antioxidant capacity of the OPN's hydroalcoholic extract is related to its composition, which is mainly composed of high-polarity antioxidant compounds such as peptides and aminoacids. However, this activity was reduced for PLA/PEG/OPN nanofibers, ranging from 36 % to 43 % (Fig. 7D). Nevertheless, the antioxidant and radical scavenging activities of PLA/PEG/OPN nanofibers increased with increasing amounts of OPN (36 % (PLA/PEG/OPN 12.5 %), 42 % (PLA/PEG/OPN 25 %), and 43 % (PLA/PEG/OPN 50 %), respectively). However, a tendency for the antioxidant activity to stabilize between the 25 and 50 % w/w OPN concentrations was noted. According to Hu et al. [31], this is due to the increased nanofibers' hydrophilicity, which consequently have better absorption, corroborating the contact angle and swelling results (Fig. 7A and C). This aspect may also be associated with the release of encapsulated OPN compounds in PLA/PEG nanofibers, which directly depends on their morphologies. This is because nanofibers with a smaller diameter (Fig. 3A) exhibit a higher surface-to-volume ratio. Such elevated ratio facilitates greater accessibility to the aqueous medium [108]. Therefore, OPN antioxidant activity was not affected even when incorporated into the PLA/PEG solution obtained by solubilization in chloroform and acetone solvents. Furthermore, the increase in antioxidant activity as a function of concentration highlighted the successful OPN encapsulation in the PLA/PEG matrix, as evidenced in the rheology (Fig. 2), FTIR (Fig. 3C) and thermal analysis results (Fig. 5). It also proved that SBS technology is an efficient method for encapsulating and protecting OPN's bioactivity.

### 3.8. Cell viability, adhesion, and proliferation tests

For nanofiber membranes to be used as dressings, they must be

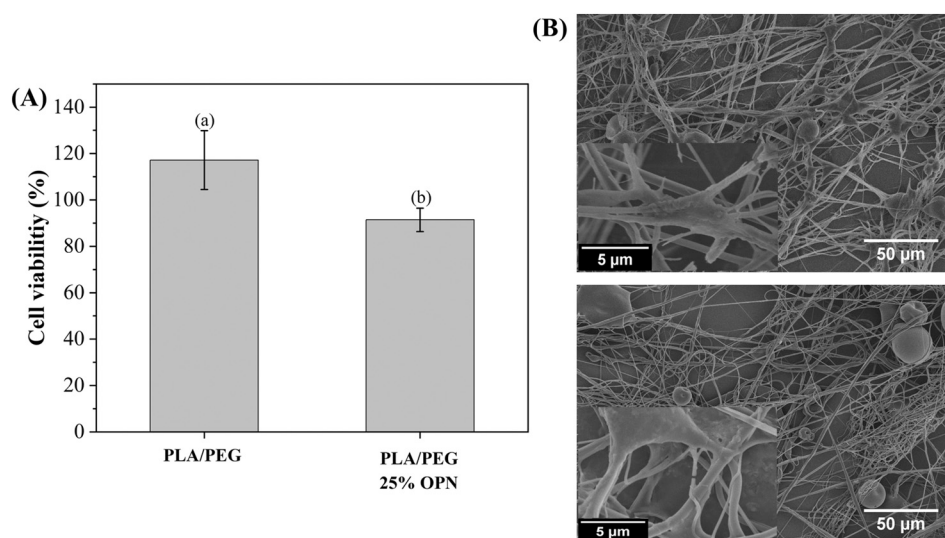


**Fig. 8.** (A) Cell viability and (B) L-929 cells' scanning electron microscopy (SEM) images after 48-hour incubation with nanofibers composed of poly(lactic acid) (PLA)/ poly(ethylene glycol) (PEG) incorporated with Ora-pro-nóbis (OPN) at a 25 % w/w concentration.

biocompatible, safe, and non-toxic to cells. Therefore, it is crucial to determine the cytotoxicity and the biocompatibility index, especially given that the matrix material for nanofiber membranes (PLA/PEG) involves using chloroform and acetone. The safety of nanofiber membranes for fibroblasts (L-929 cells) was assessed by cell viability assays and cell morphology experiment (SEM) to examine cell adhesion, as shown in Fig. 8A and B, respectively. Based on the presented results, only the PLA/PEG and PLA/PEG/OPN 25 % nanofiber membranes were evaluated for cell viability and adhesion.

As depicted in Fig. 8A, the PLA/PEG membrane's relative viability was approximately 117 %. However, the number of fibroblast cells on the 25 % PLA/PEG/OPN composite nanofiber membranes was slightly lower than that in the control nanofiber membranes (PLA/PEG). Barnhip et al. [30] attributed this to the fibers' diameter obtained and, consequently, the increase in the surface area and volume ratio. Their studies revealed that a smaller fiber diameter resulted in greater cell adhesion. This is in line with the findings of this study, where the PLA/PEG nanofibers had a smaller diameter than the PLA/PEG/OPN25% nanofibers (Fig. 3A and B).

Despite this minor reduction in cell viability in OPN-incorporated nanofiber membranes, it is essential to note that neither the polymers (PLA/PEG) nor the amount released of OPN presented cytotoxicity. This is consistent with the ISO standard 10,993-5 requirements [77], which stipulates that cell viability must be equal to or >70 % for medical devices to be considered non-toxic, suggesting nanofibers' biocompatibility.

Furthermore, SEM images were used to assess L-929 cells morphology on the nanofiber membranes after a 48-hour growth period (Fig. 8B). A high-magnification image of a single cell was incorporated into each image. The cells grown on the nanofibers exhibited morphology and characteristics specific to fibroblast cells, as reported by Lv et al. [42], who found cells with standard fusiform extension. The number of cells distributed on the 25 % PLA/PEG/OPN nanofiber appeared visually lower than those on the control nanofiber (PLA/PEG), which was consistent with the cell viability test results (Fig. 8A).

In contrast to other studies in the literature [28,30,42,57,62], which linked greater biocompatibility with the hydrophilic, the matrix in this study provided an efficient surface for adhesion (Fig. 8B) even with its hydrophobicity nature (Fig. 7A). According to Liu et al. [28], this may be linked to the nanofibers diameter reduction, which consequently increased the water penetration rate due to an increase in the nanofibers' surface-to-volume ratio and porosity. This is in line with the results presented in this study, where the PLA/PEG/OPN25% nanofibers diameter was reduced (Fig. 3B), leading to an increased WVTR rate (Fig. 7B). Therefore, these results indicated that PLA/PEG/OPN nanofiber membranes offer a comparable support to PLA/PEG nanofibers, established in the literature for used as dressings, fostering cell adhesion and proliferation, suggesting their potential use as wound dressings.

#### 4. Conclusion

PLA/PEG nanofiber membranes, incorporating various OPN concentrations (12.5, 25 and 50 % w/w), were successfully produced using SBS technology. Overall, the nanofiber membranes exhibited an average diameter ranging from 104 to 264 nm and displayed uniformly without any defects. These nanofiber membranes demonstrated thermal stability, a crucial aspect for their storage and application, especially when OPN was incorporated. OPN incorporation notably enhanced the mechanical properties, which is evident in the TS increase from 0.8 MPa for PLA/PEG to 2.0 MPa after incorporating 25 % w/w OPN. Furthermore, the PLA/PEG/OPN nanofibers offered an excellent wound healing system with advantageous features, including the establishment of an antioxidant environment (DPPH~45 %, PLA/PEG/OPN25%), a slight reduction in contact angle (109°), and enhanced moisture exchange by increasing the water vapor transmission rate (WVTR) from 2343 to 1366 g/m<sup>2</sup>/day. Significantly, in vitro viability and cell culture test

results demonstrated that both PLA/PEG and PLA/PEG/OPN (25 % w/w OPN) nanofiber membranes promoted cell adhesion, fibroblast cell attachment (L929), and cell proliferation without inducing any cytotoxic effects. Therefore, based on the results presented in this study, PLA/PEG nanofibers incorporated with OPN showed promising potential use as wound dressing applications.

Supplementary data to this article can be found online at <https://doi.org/10.1016/j.ijbiomac.2024.131365>.

#### CRedit authorship contribution statement

**Juliana Farinassi Mendes:** Writing – review & editing, Writing – original draft, Visualization, Validation, Software, Project administration, Methodology, Investigation, Formal analysis, Data curation, Conceptualization. **Marina de Lima Fontes:** Investigation, Formal analysis. **Talita Villa Barbosa:** Investigation, Formal analysis. **Rafaella T. Paschoalin:** Writing – review & editing, Resources, Investigation. **Luiz Henrique Capparelli Mattoso:** Writing – original draft, Visualization, Supervision, Funding acquisition.

#### Declaration of competing interest

The authors declare no competing financial interest.

#### Data availability

Data will be made available on request.

#### Acknowledgments

The authors would like to thank the Fundação de Amparo à Pesquisa do Estado de São Paulo–FAPESP (grant#2019/26622-4), National Council for Scientific and Technological Development CNPq, CAPES, and the Brazilian Agricultural Research Corporation (Embrapa), particularly Embrapa Instrumentação, for their support.

#### References

- T.T.T. Nguyen, C. Ghosh, S.-G. Hwang, L.D. Tran, J.S. Park, Characteristics of curcumin-loaded poly (lactic acid) nanofibers for wound healing, *J. Mater. Sci.* 48 (2013) 7125–7133, <https://doi.org/10.1007/s10853-013-7527-y>.
- J.A.A. Garcia, R.C.G. Corrêa, L. Barros, C. Pereira, R.M.V. Abreu, M.J. Alves, R. C. Calhelha, A. Bracht, R.M. Peralta, I.C.F.R. Ferreira, Phytochemical profile and biological activities of “Ora-pro-nobis” leaves (*Pereskia aculeata* Miller), an underexploited superfood from the Brazilian Atlantic Forest, *Food Chem.* 294 (2019) 302–308, <https://doi.org/10.1016/j.foodchem.2019.05.074>.
- R.T. Paschoalin, B. Traldi, G. Aydin, J.E. Oliveira, S. Rütten, L.H.C. Mattoso, M. Zenke, A. Sechi, Solution blow spinning fibres: new immunologically inert substrates for the analysis of cell adhesion and motility, *Acta Biomater.* 51 (2017) 161–174, <https://doi.org/10.1016/j.actbio.2017.01.020>.
- B. Motealleh, P. Zahedi, I. Rezaeian, M. Moghimi, A.H. Abdolghaffari, M. A. Zarandi, Morphology, drug release, antibacterial, cell proliferation, and histology studies of chamomile-loaded wound dressing mats based on electrospun nanofibrous poly( $\epsilon$ -caprolactone)/polystyrene blends, *J. Biomed. Mater. Res. Part B Appl. Biomater.* 102 (2014) 977–987, <https://doi.org/10.1002/jbm.b.33078>.
- K.N. Ferreira, R.R. Oliveira, L.R.C. Castellano, P.R.F. Bonan, O.V. Carvalho, L. Pena, J.R. Souza, J.E. Oliveira, E.S. Medeiros, Controlled release and antiviral activity of acyclovir-loaded PLA/PEG nanofibers produced by solution blow spinning, *Biomater. Adv.* 136 (2022) 212785, <https://doi.org/10.1016/j.bioadv.2022.212785>.
- M. Sharifi, S.A. Sadati, S.H. Bahrami, S.M.A. Haramshahi, Modeling and optimization of poly(lactic acid)/poly( $\epsilon$ -caprolactone)/*Nigella sativa* extract nanofibers production for skin wounds healing by artificial neural network and response surface methodology models, *Int. J. Biol. Macromol.* 253 (2023) 127227, <https://doi.org/10.1016/j.ijbiomac.2023.127227>.
- M. Bayrakci, M. Keskinates, B. Yilmaz, Antibacterial, thermal decomposition and in vitro time release studies of chloramphenicol from novel PLA and PVA nanofiber mats, *Mater. Sci. Eng. C* 122 (2021) 111895, <https://doi.org/10.1016/j.msec.2021.111895>.
- L. Moradkhannejhad, M. Abdouss, N. Nikfarjam, M.H. Shahriari, V. Heidary, The effect of molecular weight and content of PEG on in vitro drug release of electrospun curcumin loaded PLA/PEG nanofibers, *J. Drug Deliv. Sci. Technol.* 56 (2020) 101554, <https://doi.org/10.1016/j.jddst.2020.101554>.

- [9] R. Goyal, L.K. Macri, H.M. Kaplan, J. Kohn, Nanoparticles and nanofibers for topical drug delivery, *J. Control. Release* 240 (2016) 77–92, <https://doi.org/10.1016/j.jconrel.2015.10.049>.
- [10] J. González-Benito, J. Teno, G. González-Gaitano, S. Xu, M.Y. Chiang, PVDF/TiO<sub>2</sub> nanocomposites prepared by solution blow spinning: surface properties and their relation with *S. Mutans* adhesion, *Polym. Test.* 58 (2017) 21–30, <https://doi.org/10.1016/j.polymertesting.2016.12.005>.
- [11] E.S. Medeiros, G.M. Glenn, A.P. Klamczynski, W.J. Orts, L.H.C. Mattoso, Solution blow spinning: a new method to produce micro- and nanofibers from polymer solutions, *J. Appl. Polym. Sci.* 113 (2009) 2322–2330, <https://doi.org/10.1002/app.30275>.
- [12] E.S. Medeiros, L.H.C. Mattoso, E.N. Ito, K.S. Gregorski, G.H. Robertson, R. D. Offeman, D.F. Wood, W.J. Orts, S.H. Imam, Electrospun nanofibers of poly(vinyl alcohol) reinforced with cellulose nanofibrils, *J. Biobased Mater. Bioenergy* 2 (2008) 231–242, <https://doi.org/10.1166/jbmb.2008.411>.
- [13] E.S. Medeiros, L.H.C. Mattoso, R.D. Offeman, D.F. Wood, W.J. Orts, Effect of relative humidity on the morphology of electrospun polymer fibers, *Can. J. Chem.* 86 (2008) 590–599, <https://doi.org/10.1139/v08-029>.
- [14] C. Shen, J. Zhong, F. Guo, C. Zhang, C. Zhu, D. Wu, K. Chen, Curcumin-loaded polycaprolactone/carboxymethyl chitosan nanofibers with photodynamic inactivation of *Staphylococcus aureus* developed by solution blow spinning, *LWT* 186 (2023) 115261, <https://doi.org/10.1016/j.lwt.2023.115261>.
- [15] R.T. Paschoalin, N.O. Gomes, G.F. Almeida, S. Bilatto, C.S. Farinas, S.A. S. Machado, L.H.C. Mattoso, O.N. Oliveira, P.A. Raymundo-Pereira, Wearable sensors made with solution-blow spinning poly(lactic acid) for non-enzymatic pesticide detection in agriculture and food safety, *Biosens. Bioelectron.* 199 (2022) 113875, <https://doi.org/10.1016/j.bios.2021.113875>.
- [16] M.-Y. Yang, K.-C. Chang, L.-Y. Chen, A. Hu, Low-dose blue light irradiation enhances the antimicrobial activities of curcumin against *Propionibacterium acnes*, *J. Photochem. Photobiol. B Biol.* 189 (2018) 21–28, <https://doi.org/10.1016/j.jphotobiol.2018.09.021>.
- [17] J. Bang, S. Park, S.-W. Hwang, J.-K. Oh, H. Yeo, H.-J. Jin, H.W. Kwak, Biodegradable and hydrophobic nanofibrous membranes produced by solution blow spinning for efficient oil/water separation, *Chemosphere* 312 (2023) 137240, <https://doi.org/10.1016/j.chemosphere.2022.137240>.
- [18] J.E. Oliveira, L.H.C. Mattoso, W.J. Orts, E.S. Medeiros, Structural and morphological characterization of micro and nanofibers produced by electrospinning and solution blow spinning: a comparative study, *Adv. Mater. Sci. Eng.* 2013 (2013) 1–14, <https://doi.org/10.1155/2013/409572>.
- [19] A. Katoria, S. Sinha-Ray, A review on biopolymer-based fibers via electrospinning and solution blowing and their applications, *Fibers* 6 (2018) 45, <https://doi.org/10.3390/fib6030045>.
- [20] A. Kasiri, J.E. Domínguez, J. González-Benito, Morphology optimization of solution blow spun polystyrene to obtain superhydrophobic materials with high ability of oil absorption, *Polym. Test.* 91 (2020) 106859, <https://doi.org/10.1016/j.polymertesting.2020.106859>.
- [21] J. González-Benito, D. Torres, C. Ballesteros, V.M. Ruiz, J. Teno, PVDF based nanocomposites produced by solution blow spinning, structure and morphology induced by the presence of MWCNT and their consequences on some properties, *Colloid Polym. Sci.* 297 (2019) 1105–1118, <https://doi.org/10.1007/s00396-019-04530-5>.
- [22] D.D. da S. Parize, J.E. de Oliveira, T. Williams, D. Wood, R. de J. Avena-Bustillos, A.P. Klamczynski, G.M. Glenn, J.M. Marconcini, L.H.C. Mattoso, Solution blow spun nanocomposites of poly(lactic acid)/cellulose nanocrystals from Eucalyptus kraft pulp, *Carbohydr. Polym.* 174 (2017) 923–932, <https://doi.org/10.1016/j.carbpol.2017.07.019>.
- [23] J. Teno, G. González-Gaitano, J. González-Benito, Poly(ethylene-co-vinyl acetate) films prepared by solution blow spinning: surface characterization and its relation with *E. coli* adhesion, *Polym. Test.* 60 (2017) 140–148, <https://doi.org/10.1016/j.polymertesting.2017.03.020>.
- [24] M. Iorio, J. Teno, M. Nicolás, R. García-González, V.H. Peláez, G. González-Gaitano, J. González-Benito, Conformational changes on PMMA induced by the presence of TiO<sub>2</sub> nanoparticles and the processing by Solution Blow Spinning, *Colloid Polym. Sci.* 296 (2018) 461–469, <https://doi.org/10.1007/s00396-018-4268-0>.
- [25] J. Teno, G. González-Gaitano, J. González-Benito, Nanofibrous polysulfone/TiO<sub>2</sub> nanocomposites: surface properties and their relation with *E. coli* adhesion, *J. Polym. Sci. Part B Polym. Phys.* 55 (2017) 1575–1584, <https://doi.org/10.1002/polb.24404>.
- [26] J.L. Daristotle, L.W. Lau, M. Erdi, J. Hunter, A. Djoum, P. Srinivasan, X. Wu, M. Basu, O.B. Ayyub, A.D. Sandler, P. Kofinas, Sprayable and biodegradable, intrinsically adhesive wound dressing with antimicrobial properties, *Bioeng. Transl. Med.* 5 (2020), <https://doi.org/10.1002/btm2.10149>.
- [27] N. Alharbi, A. Daraei, H. Lee, M. Guthold, The effect of molecular weight and fiber diameter on the mechanical properties of single, electrospun PCL nanofibers, *Mater. Today Commun.* 35 (2023) 105773, <https://doi.org/10.1016/j.mtcomm.2023.105773>.
- [28] Y. Liu, L. Deng, C. Zhang, F. Feng, H. Zhang, Tunable physical properties of ethylcellulose/gelatin composite nanofibers by electrospinning, *J. Agric. Food Chem.* 66 (2018) 1907–1915, <https://doi.org/10.1021/acs.jafc.7b06038>.
- [29] M. Ranjbar-Mohammadi, P. Shakoori, Z. Arab-Bafarani, Design and characterization of keratin/PVA-PLA nanofibers containing hybrids of nanofibrillated chitosan/ZnO nanoparticles, *Int. J. Biol. Macromol.* 187 (2021) 554–565, <https://doi.org/10.1016/j.ijbiomac.2021.07.160>.
- [30] N. Barnthip, J. Teeka, P. Kantha, S. Teepoo, W. Damjuti, Fabrication and characterization of polycaprolactone/cellulose acetate blended nanofiber mats containing sericin and fibroin for biomedical application, *Sci. Rep.* 12 (2022) 22370, <https://doi.org/10.1038/s41598-022-26908-2>.
- [31] X. Hu, X. Wang, L. Han, S. Li, W. Zhou, Antioxidant and antimicrobial polyvinyl alcohol electrospun nanofibers containing baicalein-hydroxypropyl-β-cyclodextrin inclusion complex, *Colloids Surfaces A Physicochem. Eng. Asp.* 614 (2021) 126135, <https://doi.org/10.1016/j.colsurfa.2021.126135>.
- [32] A. Ullah, S. Ullah, M.Q. Khan, M. Hashmi, P.D. Nam, Y. Kato, Y. Tamada, I.S. Kim, Manuka honey incorporated cellulose acetate nanofibrous mats: fabrication and in vitro evaluation as a potential wound dressing, *Int. J. Biol. Macromol.* 155 (2020) 479–489, <https://doi.org/10.1016/j.ijbiomac.2020.03.237>.
- [33] Y. Han, J. Ding, J. Zhang, Q. Li, H. Yang, T. Sun, H. Li, Fabrication and characterization of polylactic acid coaxial antibacterial nanofibers embedded with cinnamaldehyde/tea polyphenol with food packaging potential, *Int. J. Biol. Macromol.* 184 (2021) 739–749, <https://doi.org/10.1016/j.ijbiomac.2021.06.143>.
- [34] Y. Zhao, Q. Lu, J. Wu, Y. Zhang, J. Guo, J. Yu, X. Shu, Q. Chen, Flexible, robust and self-peeling PLA/AgNWs nanofiber membranes with photothermally antibacterial properties for wound dressing, *Appl. Surf. Sci.* 615 (2023) 156284, <https://doi.org/10.1016/j.apsusc.2022.156284>.
- [35] C. Echeverría, A. Muñoz-Bonilla, R. Cuervo-Rodríguez, D. López, M. Fernández-García, Antibacterial PLA fibers containing thiazolium groups as wound dressing materials, *ACS Appl. Bio Mater.* 2 (2019) 4714–4719, <https://doi.org/10.1021/acsbm.9b00923>.
- [36] F.R. Beltrán, V. Lorenzo, J. Acosta, M.U. de la Orden, J. Martínez Urreaga, Effect of simulated mechanical recycling processes on the structure and properties of poly(lactic acid), *J. Environ. Manag.* 216 (2018) 25–31, <https://doi.org/10.1016/j.jenvman.2017.05.020>.
- [37] O. Avinc, A. Khoddami, Overview of poly(lactic acid) (PLA) fibre: part II: wet processing; pretreatment, dyeing, clearing, finishing, and washing properties of poly(lactic acid) Fibres, *Fibre Chem.* 42 (2010) 68–78, <https://doi.org/10.1007/s10692-010-9226-7>.
- [38] D.A. Locilento, L.A. Mercante, R.S. Andre, L.H.C. Mattoso, G.L.F. Luna, P. Brassolatti, F. de F. Anibal, D.S. Correa, Biocompatible and biodegradable electrospun nanofibrous membranes loaded with grape seed extract for wound dressing application, *J. Nanomater.* 2019 (2019) 1–11, <https://doi.org/10.1155/2019/2472964>.
- [39] M. Santoro, S.R. Shah, J.L. Walker, A.G. Mikos, Poly(lactic acid) nanofibrous scaffolds for tissue engineering, *Adv. Drug Deliv. Rev.* 107 (2016) 206–212, <https://doi.org/10.1016/j.addr.2016.04.019>.
- [40] S. Chitrattha, T. Phaechamud, Porous poly(dl-lactic acid) matrix film with antimicrobial activities for wound dressing application, *Mater. Sci. Eng. C* 58 (2016) 1122–1130, <https://doi.org/10.1016/j.msec.2015.09.083>.
- [41] F. Zou, X. Sun, X. Wang, Elastic, hydrophilic and biodegradable poly(1, 8-octanediol-co-citric acid)/polylactic acid nanofibrous membranes for potential wound dressing applications, *Polym. Degrad. Stab.* 166 (2019) 163–173, <https://doi.org/10.1016/j.polydegradstab.2019.05.024>.
- [42] Y. Lv, Z. Yu, C. Li, J. Zhou, X. Lv, J. Chen, M. Wei, J. Liu, X. Yu, C. Wang, P. Hu, Y. Liu, Gelatin-based nanofiber membranes loaded with curcumin and borneol as a sustainable wound dressing, *Int. J. Biol. Macromol.* 219 (2022) 1227–1236, <https://doi.org/10.1016/j.ijbiomac.2022.08.198>.
- [43] R.E. Elsayed, T.M. Madkour, R.A. Azzam, Tailored-design of electrospun nanofiber cellulose acetate/poly(lactic acid) dressing mats loaded with a newly synthesized sulfonamide analog exhibiting superior wound healing, *Int. J. Biol. Macromol.* 164 (2020) 1984–1999, <https://doi.org/10.1016/j.ijbiomac.2020.07.316>.
- [44] J.-L. Dewez, J.-B. Lhoest, E. Detrait, V. Berger, C.C. Dupont-Gillain, L.-M. Vincent, Y.-J. Schneider, P. Bertrand, P.G. Rouxhet, Adhesion of mammalian cells to polymer surfaces: from physical chemistry of surfaces to selective adhesion on defined patterns, *Biomaterials* 19 (1998) 1441–1445, [https://doi.org/10.1016/S0142-9612\(98\)00055-6](https://doi.org/10.1016/S0142-9612(98)00055-6).
- [45] C. Lai, Z. Zhou, L. Zhang, X. Wang, Q. Zhou, Y. Zhao, Y. Wang, X.-F. Wu, Z. Zhu, H. Fong, Free-standing and mechanically flexible mats consisting of electrospun carbon nanofibers made from a natural product of alkali lignin as binder-free electrodes for high-performance supercapacitors, *J. Power Sources* 247 (2014) 134–141, <https://doi.org/10.1016/j.jpowsour.2013.08.082>.
- [46] A. Grizzo, D.M. dos Santos, V.P.V. da Costa, R.G. Lopes, N.M. Inada, D.S. Correa, S.P. Campana-Filho, Multifunctional bilayer membranes composed of poly(lactic acid), beta-chitin whiskers and silver nanoparticles for wound dressing applications, *Int. J. Biol. Macromol.* 251 (2023) 126314, <https://doi.org/10.1016/j.ijbiomac.2023.126314>.
- [47] M.E.F. de Almeida, A.D. Corrêa, Utilização de cactáceas do gênero *Pereskia* na alimentação humana em um município de Minas Gerais, *Ciência Rural* 42 (2012) 751–756, <https://doi.org/10.1590/S0103-84782012000400029>.
- [48] Behnaz Hassanbaglou, Antioxidant activity of different extracts from leaves of *Pereskia bleo* (Cactaceae), *J. Med. Plant Res.* 6 (2012), <https://doi.org/10.5897/JMPR11.760>.
- [49] C.M. Spagnolo, R.P. Assis, I.L. Brunetti, V.L.B. Isaac, H.R.N. Salgado, M.A. Corrêa, In vitro methods to determine the antioxidant activity of caffeic acid, *Spectrochim Acta Part A Mol. Biomol. Spectrosc.* 219 (2019) 358–366, <https://doi.org/10.1016/j.saa.2019.04.025>.
- [50] T. Hatahet, M. Morille, A. Hommoss, J.M. Devoisselle, R.H. Müller, S. Bégu, Liposomes, lipid nanocapsules and smartCrystals®: a comparative study for an effective quercetin delivery to the skin, *Int. J. Pharm.* 542 (2018) 176–185, <https://doi.org/10.1016/j.ijpharm.2018.03.019>.
- [51] N. de C.C. Pinto, A.P. do N. Duque, N.R. Pacheco, R. de F. Mendes, E.V. da S. Motta, P.M.Q. Bellozi, A. Ribeiro, M.J. Salvador, E. Scio, *Pereskia aculeata*: a

- plant food with antinociceptive activity, *Pharm. Biol.* 53 (2015) 1780–1785, <https://doi.org/10.3109/13880209.2015.1008144>.
- [52] A.A. Martin, R.A. de Freitas, G.L. Sasaki, P.H.L. Evangelista, M.R. Sierakowski, Chemical structure and physical-chemical properties of mucilage from the leaves of *Pereskia aculeata*, *Food Hydrocoll.* 70 (2017) 20–28, <https://doi.org/10.1016/j.foodhyd.2017.03.020>.
- [53] F. Bonina, Flavonoids as potential protective agents against photo-oxidative skin damage, *Int. J. Pharm.* 145 (1996) 87–94, [https://doi.org/10.1016/S0378-5173\(96\)04728-X](https://doi.org/10.1016/S0378-5173(96)04728-X).
- [54] C.F.P. Sartor, V. Amaral, H.E.T. Guimarães, K.N. Barros, D.F. Felipe, L.E. R. Cortez, Estudo da ação cicatrizante das folhas de *Pereskia aculeata*, *Saúde e Pesqui.* 3 (2010) 149–154.
- [55] N. Lucyszyn, L. Ono, A.F. Lubambo, M.A. Woehl, C.V. Sens, C.F. de Souza, M. R. Sierakowski, Physicochemical and in vitro biocompatibility of films combining reconstituted bacterial cellulose with arabinogalactan and xyloglucan, *Carbohydr. Polym.* 151 (2016) 889–898, <https://doi.org/10.1016/j.carbpol.2016.06.027>.
- [56] M.N. Uddin, M. Mohebbullah, S.M. Islam, M.A. Uddin, M. Jobaer, Nigella/honey/garlic/olive oil co-loaded PVA electrospun nanofibers for potential biomedical applications, *Prog. Biomater.* 11 (2022) 431–446, <https://doi.org/10.1007/s40204-022-00207-5>.
- [57] I.C.O. Neves, S.H. Silva, N.L. Oliveira, A.M.T. Lago, N. Ng, A. Sultani, P. H. Campelo, L.A.A. Veríssimo, J.V. de Resende, M.A. Rogers, Effect of carrier oil on  $\alpha$ -tocopherol encapsulation in ora-pro-nobis (*Pereskia aculeata* Miller) mucilage-when protein isolate microparticles, *Food Hydrocoll.* 105 (2020) 105716, <https://doi.org/10.1016/j.foodhyd.2020.105716>.
- [58] AOCS, *Official Methods and Recommended Practices of the American Oil Chemists' Society*, 2008.
- [59] AOAC Official Method 934.01, *Official Method 934.01*, 17th Editi, Association of Analytical Communities, Gaithersburg, 2006.
- [60] ABNT, NBR 7989: Pulp and Wood – Determination of Acid-insoluble Lignin, 2010.
- [61] L. Rebenfeld, The chemistry of Wood. B. L. Browning, *Science* (80) 142 (1963) 1564, <https://doi.org/10.1126/science.142.3599.1564-a>.
- [62] C.A. White, Wood and celluloses: industrial utilization, biotechnology, structure and properties edited by J. F. Kennedy, G. O. Phillips and P. A. Williams, Ellis Horwood, Chichester, 1987. pp. xiv + 664, price £69-50. ISBN 0-7458-01 13-7, *Br. Polym. J.* 20 (1988) 300–300. doi:<https://doi.org/10.1002/pi.4980200327>.
- [63] R. Casasola, N.L. Thomas, A. Trybala, S. Georgiadou, Electrospun poly lactic acid (PLA) fibres: effect of different solvent systems on fibre morphology and diameter, *Polymer (Guildf.)* 55 (2014) 4728–4737, <https://doi.org/10.1016/j.polymer.2014.06.032>.
- [64] T. Casalini, F. Rossi, A. Castrovinci, G. Perale, A perspective on polylactic acid-based polymers use for nanoparticles synthesis and applications, *Front. Bioeng. Biotechnol.* 7 (2019), <https://doi.org/10.3389/fbioe.2019.00259>.
- [65] T. Riley, C.R. Heald, S. Stolnik, M.C. Garnett, L. Illum, S.S. Davis, S.M. King, R. K. Heenan, S.C. Purkiss, R.J. Barlow, P.R. Gellert, C. Washington, Core–Shell structure of PLA–PEG nanoparticles used for drug delivery, *Langmuir* 19 (2003) 8428–8435, <https://doi.org/10.1021/la020911h>.
- [66] J.F. Mendes, L.B. Norcino, T.Q. Corrêa, T.V. Barbosa, R.T. Paschoalin, L.H. C. Mattoso, Obtaining poly (lactic acid) nanofibers encapsulated with peppermint essential oil as potential packaging via solution-blow-spinning, *Int. J. Biol. Macromol.* 230 (2023) 123424, <https://doi.org/10.1016/j.ijbiomac.2023.123424>.
- [67] ASTM E2550, Standard Test Method for Thermal Stability by Thermogravimetry 5, 2021, <https://doi.org/10.1520/E2550-21>.
- [68] S. Fahimirad, P. Satei, A. Ganji, H. Abtahi, Wound healing capability of the double-layer polycaprolactone/polyvinyl alcohol-chitosan lactate electrospun nanofiber incorporating *Echinacea purpurea* extract, *J. Drug Deliv. Sci. Technol.* 87 (2023) 104734, <https://doi.org/10.1016/j.jddst.2023.104734>.
- [69] ASTM E96, *Standard Test Methods for Water Vapor Transmission of Materials*, 2016.
- [70] H.A.S. Al-Naymi, E. Mahmoudi, M.M. Kamil, Y.Q. Almajidi, M.H. Al-Musawi, V. Mohammadzadeh, M. Ghorbani, F. Mortazavi Moghadam, A novel designed nanofibrous mat based on hydroxypropyl methyl cellulose incorporating mango peel extract for potential use in wound care system, *Int. J. Biol. Macromol.* 259 (2024) 129159, <https://doi.org/10.1016/j.ijbiomac.2023.129159>.
- [71] G. Zhong, M. Qiu, J. Zhang, F. Jiang, X. Yue, C. Huang, S. Zhao, R. Zeng, C. Zhang, Y. Qu, Fabrication and characterization of PVA@PLA electrospinning nanofibers embedded with *Bletilla striata* polysaccharide and Rosmarinic acid to promote wound healing, *Int. J. Biol. Macromol.* 234 (2023) 123693, <https://doi.org/10.1016/j.ijbiomac.2023.123693>.
- [72] S. Habibi, T. Mohammadi, A.A. Asadi, Tailoring polyethylene oxide-modified cross-linked chitosan/PVA nanofibrous membranes: burn dressing scaffold developed for mupirocin release, *Int. J. Biol. Macromol.* 258 (2024) 128983, <https://doi.org/10.1016/j.ijbiomac.2023.128983>.
- [73] W. Zhang, H. Liu, L. Yan, X. Mei, Z. Hou, Combining emulsion electrospinning with surface functionalization to fabricate multistructural PLA/CS@ZIF-8 nanofiber membranes toward pH-responsive dual drug delivery, *Int. J. Biol. Macromol.* 253 (2023) 126506, <https://doi.org/10.1016/j.ijbiomac.2023.126506>.
- [74] J. Ding, V. Dwibedi, H. Huang, Y. Ge, Y. Li, Q. Li, T. Sun, Preparation and antibacterial mechanism of cinnamaldehyde/tea polyphenol/poly(lactic acid) coaxial nanofiber films with zinc oxide sol to *Shewanella putrefaciens*, *Int. J. Biol. Macromol.* 237 (2023) 123932, <https://doi.org/10.1016/j.ijbiomac.2023.123932>.
- [75] H. Zhang, Q. Zhai, X. Guan, Q. Zhen, X. Qian, Tri-layered bicomponent microfilament composite fabric for highly efficient cold protection, *Small* 19 (2023), <https://doi.org/10.1002/sml.202303820>.
- [76] L. da Silva Uebel, D. Angelica Schmatz, S. Goettmens Kuntzler, C. Lima Dora, A. Luiza Muccillo-Baisch, J. Alberto Vieira Costa, M. Greque de Moraes, Quercetin and curcumin in nanofibers of polycaprolactone and poly(hydroxybutyrate-co-hydroxyvalerate): assessment of in vitro antioxidant activity, *J. Appl. Polym. Sci.* 133 (2016), <https://doi.org/10.1002/app.43712>.
- [77] ISO 10993-5, *Biological Evaluation of Medical Devices — Part 5: Tests for In Vitro Cytotoxicity*, 2019.
- [78] N.L. Oliveira, A.A. Rodrigues, I.C. Oliveira Neves, A.M. Teixeira Lago, S. V. Borges, J.V. de Resende, Development and characterization of biodegradable films based on *Pereskia aculeata* Miller mucilage, *Ind. Crop. Prod.* 130 (2019) 499–510, <https://doi.org/10.1016/j.indcrop.2019.01.014>.
- [79] F.A. Lima Junior, M.C. Conceição, J. Vilela de Resende, L.A. Junqueira, C. Pereira, M.E. Torres Prado, Response surface methodology for optimization of the mucilage extraction process from *Pereskia aculeata* Miller, *Food Hydrocoll.* 33 (2013) 38–47, <https://doi.org/10.1016/j.foodhyd.2013.02.012>.
- [80] E.R.P. Keijsers, G. Yilmaz, J.E.G. van Dam, The cellulose resource matrix, *Carbohydr. Polym.* 93 (2013) 9–21, <https://doi.org/10.1016/j.carbpol.2012.08.110>.
- [81] D. Jubinville, C. Tzoganakis, T.H. Mekonnen, Recycled PLA – Wood flour based biocomposites: effect of wood flour surface modification, PLA recycling, and maleation, *Constr. Build. Mater.* 352 (2022) 129026, <https://doi.org/10.1016/j.conbuildmat.2022.129026>.
- [82] G.C. Dadol, A. Kilic, L.D. Tijjng, K.J.A. Lim, L.K. Cabatingan, N.P.B. Tan, E. Stojanovska, Y. Polat, Solution blow spinning (SBS) and SBS-spun nanofibers: materials, methods, and applications, *Mater. Today Commun.* 25 (2020) 101656, <https://doi.org/10.1016/j.mtcomm.2020.101656>.
- [83] J. Song, Z. Li, H. Wu, Blowspinning: a new choice for nanofibers, *ACS Appl. Mater. Interfaces* 12 (2020) 33447–33464, <https://doi.org/10.1021/acsmi.0c05740>.
- [84] A.K. Khan, S. Kaleem, F. Pervaiz, T.A. Sherazi, S.A. Khan, F.A. Khan, T. Jamshaid, M.I. Umar, W. Hassan, M. Ijaz, G. Murtaza, Antibacterial and wound healing potential of electrospun PVA/MMT nanofibers containing root extract of *Berberis lycium*, *J. Drug Deliv. Sci. Technol.* 79 (2023) 103987, <https://doi.org/10.1016/j.jddst.2022.103987>.
- [85] S. Alipplakkotte, S. Kumar, L. Sreejith, Fabrication of PLA/Ag nanofibers by green synthesis method using *Morinda charantia* fruit extract for wound dressing applications, *Colloids Surface A Physicochem. Eng. Asp.* 529 (2017) 771–782, <https://doi.org/10.1016/j.colsurfa.2017.06.066>.
- [86] J.L. de Oliveira, Use of the leaf and material extracted from the ora-pro-nobis leaf (*Pereskia aculeata* Miller) in the removal of Cd<sup>2+</sup> and Pb<sup>2+</sup> ions from aqueous solutions., 2019.
- [87] S. Tan, A. Ebrahimi, T. Langrish, Smart release-control of microencapsulated ingredients from milk protein tablets using spray drying and heating, *Food Hydrocoll.* 92 (2019) 181–188, <https://doi.org/10.1016/j.foodhyd.2019.02.006>.
- [88] J. Andrade, C.G. Pereira, J.C. de Almeida Junior, C.C.R. Viana, L.N. de O. Neves, P.H.F. da Silva, M.J.V. Bell, V. de C. dos Anjos, FTIR-ATR determination of protein content to evaluate whey protein concentrate adulteration, *LWT* 99 (2019) 166–172, <https://doi.org/10.1016/j.lwt.2018.09.079>.
- [89] M.C. Conceição, L.A. Junqueira, K.C. Guedes Silva, M.E.T. Prado, J.V. de Resende, Thermal and microstructural stability of a powdered gum derived from *Pereskia aculeata* Miller leaves, *Food Hydrocoll.* 40 (2014) 104–114, <https://doi.org/10.1016/j.foodhyd.2014.02.015>.
- [90] S. Singh, H. Singh, T. Karthick, P. Tandon, V. Prasad, Phase transition analysis of V-shaped liquid crystal: combined temperature-dependent FTIR and density functional theory approach, *Spectrochim. Acta Part A Mol. Biomol. Spectrosc.* 188 (2018) 561–570, <https://doi.org/10.1016/j.saa.2017.07.043>.
- [91] S. Brunet, J. Aufrere, F. El Babili, I. Fouraste, H. Hoste, The kinetics of exsheathment of infective nematode larvae is disturbed in the presence of a tannin-rich plant extract (sainfoin) both in vitro and in vivo, *Parasitology* 134 (2007) 1253–1262, <https://doi.org/10.1017/S0031182007002533>.
- [92] A. Mercê, Complexes of arabinogalactan of *Pereskia aculeata* and Co<sup>2+</sup>, Cu<sup>2+</sup>, Mn<sup>2+</sup>, and Ni<sup>2+</sup>, *Bioresour. Technol.* 76 (2001) 29–37, [https://doi.org/10.1016/S0960-8524\(00\)00078-X](https://doi.org/10.1016/S0960-8524(00)00078-X).
- [93] F. Carrasco, J. Cailloux, P.E. Sánchez-Jiménez, M.L. Maspocho, Improvement of the thermal stability of branched poly(lactic acid) obtained by reactive extrusion, *Polym. Degrad. Stab.* 104 (2014) 40–49, <https://doi.org/10.1016/j.polymdegradstab.2014.03.026>.
- [94] A.N. Frone, S. Berlioz, J.-F. Chailan, D.M. Panaitecu, Morphology and thermal properties of PLA–cellulose nanofibers composites, *Carbohydr. Polym.* 91 (2013) 377–384, <https://doi.org/10.1016/j.carbpol.2012.08.054>.
- [95] J.E. Karbowiczek, D.P. Ura, U. Stachewicz, Nanoparticles distribution and agglomeration analysis in electrospun fiber based composites for desired mechanical performance of poly(3-hydroxybutyrate-co-3-hydroxyvalerate) (PHBV) scaffolds with hydroxyapatite (HA) and titanium dioxide (TiO<sub>2</sub>) towards me, *Compos. Part B Eng.* 241 (2022) 110011, <https://doi.org/10.1016/j.compositesb.2022.110011>.
- [96] M. Tarmizie Hassim, M.N. Prabhakar, J. Song, Design of Core-Shell Poly(lactic Acid) (PLA) electrospun nanofibers as potential healing carriers, *Compos. Part A Appl. Sci. Manuf.* 173 (2023) 107661, <https://doi.org/10.1016/j.compositesa.2023.107661>.
- [97] R.L. Dahlin, F.K. Kasper, A.G. Mikos, Polymeric nanofibers in tissue engineering, *Tissue Eng. Part B Rev.* 17 (2011) 349–364, <https://doi.org/10.1089/ten.teb.2011.0238>.

- [98] V. Perez-Puyana, M. Jiménez-Rosado, A. Romero, A. Guerrero, Development of PVA/gelatin nanofibrous scaffolds for tissue engineering via electrospinning, *Mater. Res. Express*. 5 (2018) 035401, <https://doi.org/10.1088/2053-1591/aab164>.
- [99] P. Zhu, Y. Wang, X. Zhang, Preparation and characterization of electrospun nanofibre membranes incorporated with an ethanol extract of *Capparis spinosa* L. as a potential packaging material, *Food Packag. Shelf Life* 32 (2022) 100851, <https://doi.org/10.1016/j.fpsl.2022.100851>.
- [100] J.R. Dias, P.L. Granja, P.J. Bartolo, Advances in electrospun skin substitutes, *Prog. Mater. Sci.* 84 (2016) 314–334, <https://doi.org/10.1016/j.pmatsci.2016.09.006>.
- [101] J. Yin, L. Xu, A. Ahmed, Batch preparation and characterization of electrospun porous polylactic acid-based nanofiber membranes for antibacterial wound dressing, *Adv. Fiber Mater.* 4 (2022) 832–844, <https://doi.org/10.1007/s42765-022-00141-y>.
- [102] P. Zahedi, I. Rezaeian, S.-O. Ranaei-Siadat, S.-H. Jafari, P. Supaphol, A review on wound dressings with an emphasis on electrospun nanofibrous polymeric bandages, *Polym. Adv. Technol.* 21 (2010) 77–95, <https://doi.org/10.1002/pat.1625>.
- [103] X. Chen, X. Wang, S. Wang, X. Zhang, J. Yu, C. Wang, Mussel-inspired polydopamine-assisted bromelain immobilization onto electrospun fibrous membrane for potential application as wound dressing, *Mater. Sci. Eng. C* 110 (2020) 110624, <https://doi.org/10.1016/j.msec.2019.110624>.
- [104] G. Jiang, K. Ramachandraiah, C. Zhao, Advances in the development and applications of nanofibers in meat products, *Food Hydrocoll.* 146 (2024) 109210, <https://doi.org/10.1016/j.foodhyd.2023.109210>.
- [105] L. Souza, L. Caputo, I. Inchausti De Barros, F. Fratianni, F. Nazzaro, V. De Feo, *Pereskia aculeata* Muller (Cactaceae) leaves: chemical composition and biological activities, *Int. J. Mol. Sci.* 17 (2016) 1478, <https://doi.org/10.3390/ijms17091478>.
- [106] R. Hoff, H. Dagher, C.T.P. Deolindo, A.P.Z. de Melo, J. Durigon, Phenolic compounds profile and main nutrients parameters of two underestimated non-conventional edible plants: *Pereskia aculeata* Mill. (ora-pro-nóbis) and *Vitex megapotamica* (Spreng.) Moldenke (tarumã) fruits, *Food Res. Int.* 162 (2022) 112042, <https://doi.org/10.1016/j.foodres.2022.112042>.
- [107] C.Y. Takeiti, G.C. Antonio, E.M.P. Motta, F.P. Collares-Queiroz, K.J. Park, Nutritive evaluation of a non-conventional leafy vegetable (*Pereskia aculeata* Miller), *Int. J. Food Sci. Nutr.* 60 (2009) 148–160, <https://doi.org/10.1080/09637480802534509>.
- [108] B. Talib Al-Sudani, A. Khoshkalampour, M.M. Kamil, M.H. Al-Musawi, V. Mohammadzadeh, S. Ahmadi, M. Ghorbani, A novel antioxidant and antimicrobial food packaging based on Eudragit®/collagen electrospun nanofiber incorporated with bitter orange peel essential oil, *LWT* 193 (2024) 115730, <https://doi.org/10.1016/j.lwt.2024.115730>.